Extended-soft-core Baryon-Baryon ESC16 model IV. $S = -3$ and $S = -4$ Hyperon-hyperon Interactions *

M.M. Nagels

Institute of Mathematics, Astrophysics, and Particle Physics
University of Nijmegen, The Netherlands

Th.A. Rijken

Institute of Mathematics, Astrophysics, and Particle Physics
University of Nijmegen, The Netherlands and

Nishina Center for Accelerator-Based Science,
Institute for Physical and Chemical Research (RIKEN). Wako, Saitama, 351-0198, Japan

Y. Yamamoto

Nishina Center for Accelerator-Based Science,
Institute for Physical and Chemical Research (RIKEN). Wako, Saitama, 351-0198, Japan

Abstract

Background: This paper presents the Extended-Soft-Core (ESC) potentials ESC16 for baryon-baryon (BB) channels with total strangeness $S = -3, -4$. For these channels no experimental scattering data exist, apart from very recently measured preliminary correlations. Also there is no information from hypernuclei or hyperonic matter.

Purpose: The aim is to calculate the predictions of the ESC16 model for the $S = -3, -4$ BB channels.

Methods: The potential models for $S = -3, -4$ are based on SU(3) extensions of potential models for the $S = 0, -1$ and $S = -2$ sectors, which are fitted to experimental data. Flavor SU(3) symmetry is broken 'kinematically' by the masses of the baryons and the mesons. The fit to the $S = 0, -1$ sectors provides the necessary constraints to fix all free parameters, *i.e.* baryon-baryon-meson (BBM) couplings and cut-off masses. The $S = -2$ systems are constrained by the $\Delta B_{\Lambda\Lambda}$ value from the Nagara event, and the requirement of $U_\Xi \approx -10$ MeV.

Results: Various properties of the potentials are illustrated by giving results for scattering lengths, bound states, and phase-parameters.

Conclusions: No $\Xi\Xi, \Xi\Lambda, \Xi\Sigma$ bound states are predicted by the ESC16 model.

* Published in Phys. Rev. C **108**, 024003 (2023).
This preprint version contains the extra tables IXX, XX, and XXI.

I. INTRODUCTION

In this paper we present the results of the ESC16-model for channels with total strangeness $S = -3, -4$. This is a further SU(3) generalization of the ESC16 models on NN [1], YN [2], and YY [3] for baryon-baryon channels, which are henceforth referred to as paper I, II, and III respectively. A similar approach has been performed in [4], where the Nijmegen soft-core one-boson-exchange (OBE) interactions NSC97a-f for baryon-baryon (BB) systems for $S = -2, -3, -4$ were presented.

This paper forms the completion of the study of baryon-baryon interactions with the ESC-interactions, comprising all $\{8\} \otimes \{8\}$ channels, *i.e.* all strangeness S=(0,-1,-2,-3,-4) channels. The basis of this work is broken SU(3) symmetry and the NN, YN, YY-data. In this paper we show the S=-3,-4 results for the ESC16 model, which can be considered being typical for this approach to the BB-interactions. (For results and review of former versions ESC04 and ESC08 as well as applications to hypernuclei for S=(0,-1,-2) see Ref. [5].)

The OBE-models NSC97 [4] and ESC-models are the first models for which the $S < -2$ interactions contain no free parameters. Compared to NSC97 the overall description of the BB-interaction in the ESC models is clearly an improvement. In the ESC models the $S = 0, -1, -2$ interactions are fitted very succesfully to the two-body scattering data. For S=-2 there is a difficulty with (i) the $\Xi^- p$-correlations found in the ALICE-experiment at CERN [6–8], and (ii) the J-PARC/E05 data on ${}^{12}_{\Xi}$Be [9]. This hints at an incompleteness of the BB-interactions in ESC04, ESC08, and ESC16. To account for this in the ESC16*(A,B) versions SU(3) symmetric contact terms have been added.

After the Nijmegen work [4] all BB-channels have been studied also in the framework of the resonating-group method (RGM) using the SU(6) quark model [10]. Furthermore in the last years there are also studies of the S=-3,-4 systems using BB-interactions from LQCD [11, 12], and recently also results for S=-3,-4 have been given from BB-interactions from chiral-effective-field-theory [13].

For the $S = -3, -4$ channels virtually no experimental scattering information is available, except preliminary $\Xi^-\Xi^-$ and $\Xi^-\Lambda$ correlation data [14]. Also the information from hypernuclei is non-existent. For $S = -2$ there are data on double $\Lambda\Lambda$-hypernuclei, which became very much improved by the observation of the Nagara-event [15]. This event indicates that the $\Lambda\Lambda$-interaction is rather weak, in contrast to the estimates based on the older experimental observations [16, 17]. This has always been a characteristic feature of the Nijmegen soft-core models. The ESC16 model describes all experimental information on the $S = 0, -1, -2$ systems, two-body scattering and hypernuclei, very satisfactorily. An exception is the (weakly) repulsive Ξ-nucleus interaction, which is attractive experimentally. This is repaired with ESC16*(A,B).

Recently more Ξ-hypernuclei have been studied and observed [18–20], also indicating that the Ξ-nucleus interaction is attractive and the $\Xi N - \Lambda\Lambda$ coupling is weak [21].

Also, the ESC models are rather in accordance with QCD, see [1–3, 22, 23] for an exposition of the arguments. Therefore, the predictions for the $S = -3, -4$-channels can be expected to be realistic.

The study of strangeness-rich systems in astrophysics is an important topic in the last sixty years with many contributions. We refer to the (general) review papers [24, 25] for references. In particular, the Λ-hyperon-puzzle in neutron star matter [26] is reviewed in [25]. Strangeness-rich systems can be exotic multi-quark systems consisting of up (u), down (d), and strange (s) quarks; like the elusive H dibaryon, a 6-quark $uuddss$ system predicted by

Jaffe [27]. But they can also simply be bound states of nucleons (N), hyperons ($Y = \Lambda, \Sigma$), and cascades (Ξ). In order to get a better handle on the latter possibility, we are in need of potential models which describe all possible interactions between nucleons, hyperons, and cascades.

In the virtual absence of experimental information for S=-3,-4, we assume that the potentials obey (broken) flavor SU(3) symmetry. As in papers I-III, the S=-3,-4 potentials are parametrized in terms of meson-baryon-baryon, and meson-pair-baryon-baryon couplings and gaussian form factors. This enables us to include in the interaction one-boson-exchange (OBE), two-pseudoscalar-exchange (TME), and meson-pair-exchange (MPE), without any new parameters. All parameters have been fixed by a simultaneous fit to the NN and YN data, scattering and hypernuclear, see I and II. Each $NN \oplus YN$-model leads to a YY-model in a well defined way. SU(3) symmetry allows us to define all coupling constants needed to describe the multi-strange interactions in the baryon-baryon channels occurring in $\{8\} \otimes \{8\}$. In all ESC models it is assumed that the coupling constants, apart from meson-mixing, are SU(3)-symmetric. The success of the ESC models suggests that for the coupling constants deviations from SU(3) symmetry are small.

In paper III new phenomenological gaussian SU(3) symmetric two-body BB potentials are introduced in addition to the meson- and meson-pair-exchanges to investigate the possible incompleteness of the ESC-interactions considered thus far in the ESC models. The motivation for this are the recent S=-2 hypernuclei experimental observations [9, 28, 29] and G-matrix calculations [30]. Also, ESC16 fails to describe the $\Xi^- p$-correlations found in the ALICE-experiment at CERN [6, 8]. Then, fitting to the $NN \oplus YN \oplus YY$ data resulted in good BB well-depths. In this paper we include the $S = -3, -4$ results for ESC16, and the effective range parameters for the two variants ESC16*(A) and (B) [3].

Most of the details on the SU(3) description are well known, and in particular for baryon-baryon scattering they can be found in papers I-III, and e.g. [31, 32]. So, here we restrict ourselves to a minimal exposition of these matters, necessary for the readability of this paper.

The contents of this paper is as follows. In Sec. II the $S = -3, -4$ thresholds are displayed and the multi-channel description is reviewed. Furthermore, for completeness we repeat the SU(3)-symmetric interaction Lagrangian describing the interaction vertices between mesons and members of the $J^P = (1/2)^+$ baryon octet, and define their coupling constants. We then identify the various channels which occur in the $S = -3, -4$ baryon-baryon systems. We describe the R-conjugation operation which is useful for the comparison of the $(\Lambda\Xi, \Sigma\Xi)$- and the $(\Lambda N, \Sigma N)$-potentials. In Sec. III the numerical values of the used baryon masses and of the thresholds momenta are listed. In Sec. IV the meson- and meson-pair baryon-baryon couplings are addressed. In Sec. V the results for the multi-channel effective-range parameters, partial wave phaseshifts and inelasticity parameters are given, and possible bound-states are considered. In Sec. VI the paper is concluded with a short discussion and summary.

In Appendix A the SU(3)-irreps and baryon-baryon Isospin-states are displayed. In Appendix B tables with the OBE meson coupling constants, and in Appendix C the meson-pair couplings MPE for the models ESC16 and ESC16$\star(A, B)$ are given. In Appendix D tables with the coupled-channel phase parameters are shown for model ESC16.

II. CHANNELS, POTENTIALS, AND SU(3) SYMMETRY

A. Multi-channel Formalism

For the kinematics and the definition of the amplitudes, we refer to paper II of this series. Similar material can be found in [32]. Also, in paper I the derivation of the Lippmann-Schwinger equation in the context of the relativistic two-body equation is described.

On the physical particle basis, there are four charge channels:

$$\begin{aligned}
q=+1: &\quad \Sigma^+\Xi^0 \to \Sigma^+\Xi^0,\\
q=\ 0: &\quad (\Lambda\Xi^0, \Sigma^0\Xi^0, \Sigma^+\Xi^-) \to (\Lambda\Xi^0, \Sigma^0\Xi^0, \Sigma^+\Xi^-)\ ;\ \Xi^0\Xi^0 \to \Xi^0\Xi^0,\\
q=-1: &\quad (\Lambda\Xi^-, \Sigma^0\Xi^-, \Sigma^-\Xi^0) \to (\Lambda\Xi^-, \Sigma^0\Xi^-, \Sigma^-\Xi^0)\ ;\ \Xi^0\Xi^- \to \Xi^0\Xi^-,\\
q=-2: &\quad \Sigma^-\Xi^- \to \Sigma^-\Xi^-\ ;\ \Xi^-\Xi^- \to \Xi^-\Xi^-.
\end{aligned} \tag{2.1}$$

We note here that in strong interactions S is conserved and hence in the q=-1,-2 channels there is no coupling of the $\Xi\Xi$-channels in (2.1) with the others.

Like in [31, 32] and in papers I-III, the potentials are calculated on the isospin basis. For $S=-3,-4$ hyperon-hyperon systems there are three isospin channels:

$$\begin{aligned}
Y=-1, S=-3, I=1/2: &\quad (\Lambda\Xi, \Sigma\Xi \to \Lambda\Xi, \Sigma\Xi),\\
Y=-1, S=-3, I=3/2: &\quad (\Sigma\Xi \to \Sigma\Xi),\\
Y=-2, S=-4, I=0,1: &\quad (\Xi\Xi \to \Xi\Xi).
\end{aligned} \tag{2.2}$$

The relation between the charge (Q), isospin (I) and hypercharge (Y) is given by the Gell-Mann-Nishijima relation $Q = Y/2 + I_3$, where in terms of the baryon number (B) and strangeness (S) the hypercharge Y=B+S.

The two-particle thresholds in the YY-channels for S=-3,-4 are shown in Fig. 1. For $\Lambda\Xi$ at the $\Sigma\Xi$ and $\Lambda\Xi^*$ thresholds the (average) p_Λ laboratory momenta are indicated. Similarly for $\Sigma\Xi$ the p_Σ at the $\Sigma\Xi^*$ threshold. For the $\Xi\Xi$ at the $\Xi\Xi^\star$ threshold p_Ξ is shown. Here, only the $J^P = 1/2^+$ octet and $J^P = 3/2^+$ decuplet baryons are considered.

For the kinematics of the reactions and the various thresholds, see [31]. In this work we do not solve the Lippmann-Schwinger equation, but the multi-channel Schrödinger equation in configuration space, completely analogous to [32]. The multi-channel Schrödinger equation for the configuration-space potential is derived from the Lippmann-Schwinger equation through the standard Fourier transform, and the equation for the radial wave function is found to be of the form [32]

$$u''_{l,j} + (p_i^2\delta_{i,j} - A_{i,j})u_{l,j} - B_{i,j}u'_{l,j} = 0, \tag{2.3}$$

where $A_{i,j}$ contains the potential, nonlocal contributions, and the centrifugal barrier, while $B_{i,j}$ is only present when non-local contributions are included. The solution in the presence of open and closed channels is given, for example, in Ref. [33]. The inclusion of the Coulomb interaction in the configuration-space equation is well known and included in the evaluation of the scattering matrix. The Coulomb interaction is present only in the channels $\Sigma^+\Xi^-$ and $\Xi^-\Xi^-$.

Obviously, the potentials on the particle basis for the $Y=-2$ channels are given by the $I=0,1$ $\Xi\Xi$-potential on the isospin basis. For $Y=-1$ channels the potentials are related to the potentials on the isospin basis by an isospin rotation. Ordering the channels in the $q=0$

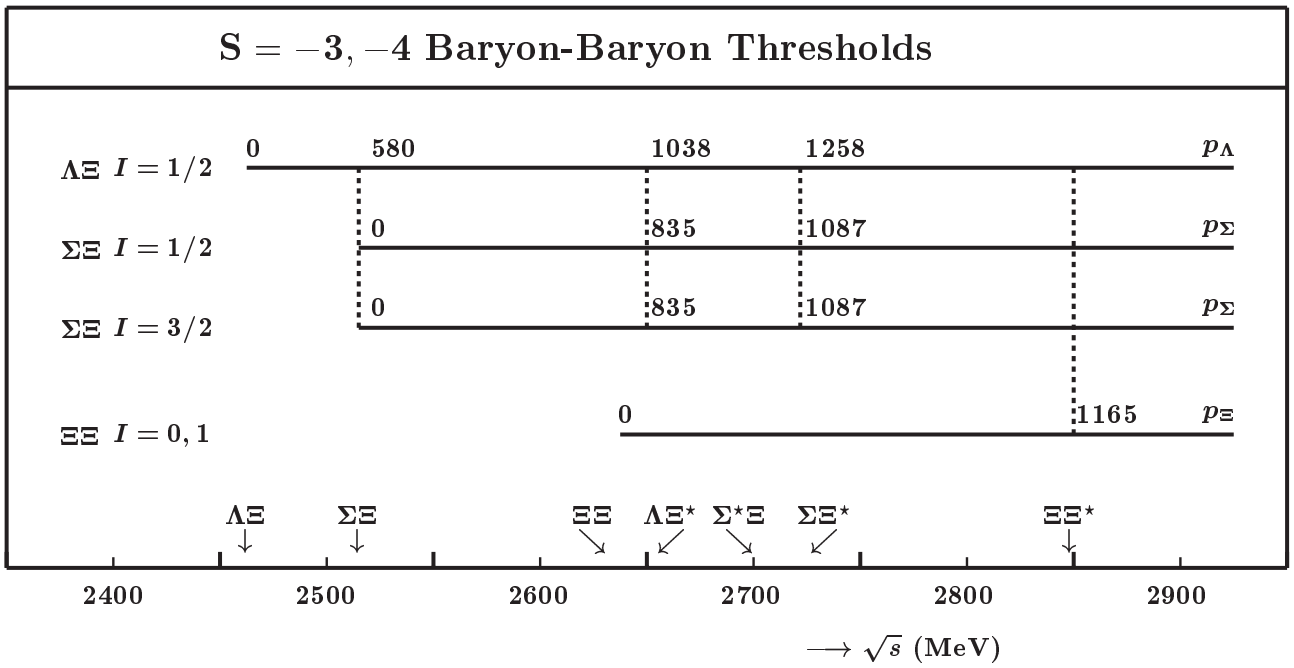

FIG. 1: Thresholds in YY-channels for $S = -3, -4$. The laboratory threshold momenta p_Λ, p_Σ and p_Ξ are given in GeV/c^2.

sector according to increasing rest mass $(\Lambda\Xi^0, \Sigma^0\Xi^0, \Sigma^+\Xi^-)$ one obtains in channel space the potential matrix , $V_{ab}(I) \equiv V_{a,\Xi;b,\Xi}(I)$, with $a, b \equiv \Lambda, \Sigma$,

$$V(q=0, Y=-1) = \begin{pmatrix} V_{\Lambda\Lambda}(\frac{1}{2}) & -\sqrt{\frac{1}{3}}V_{\Lambda\Sigma} & \sqrt{\frac{2}{3}}V_{\Lambda\Sigma} \\ -\sqrt{\frac{1}{3}}V_{\Lambda\Sigma} & \frac{1}{3}\left[V_{\Sigma\Sigma}(\frac{1}{2}) + 2V_{\Sigma\Sigma}(\frac{3}{2})\right] & \frac{\sqrt{2}}{3}\left[-V_{\Sigma\Sigma}(\frac{1}{2}) + V_{\Sigma\Sigma}(\frac{3}{2})\right] \\ \sqrt{\frac{2}{3}}V_{\Lambda\Sigma} & \frac{\sqrt{2}}{3}\left[-V_{\Sigma\Sigma}(\frac{1}{2}) + V_{\Sigma\Sigma}(\frac{3}{2})\right] & \frac{1}{3}\left[2V_{\Sigma\Sigma}(\frac{1}{2}) + V_{\Sigma\Sigma}(\frac{3}{2})\right] \end{pmatrix}, \quad (2.4)$$

and for $q = -1$ we have now the ordering $(\Lambda\Xi^-, \Sigma^-\Xi^0, \Sigma^0\Xi^-)$, and we get for the potential matrix

$$V(q=-1, Y=-1) = \begin{pmatrix} V_{\Lambda\Lambda}(\frac{1}{2}) & -\sqrt{\frac{2}{3}}V_{\Lambda\Sigma} & \sqrt{\frac{1}{3}}V_{\Lambda\Sigma} \\ -\sqrt{\frac{2}{3}}V_{\Lambda\Sigma} & \frac{1}{3}\left[2V_{\Sigma\Sigma}(\frac{1}{2}) + V_{\Sigma\Sigma}(\frac{3}{2})\right] & \frac{\sqrt{2}}{3}\left[-V_{\Sigma\Sigma}(\frac{1}{2}) + V_{\Sigma\Sigma}(\frac{3}{2})\right] \\ \sqrt{\frac{1}{3}}V_{\Lambda\Sigma} & \frac{\sqrt{2}}{3}\left[-V_{\Sigma\Sigma}(\frac{1}{2}) + V_{\Sigma\Sigma}(\frac{3}{2})\right] & \frac{1}{3}\left[V_{\Sigma\Sigma}(\frac{1}{2}) + 2V_{\Sigma\Sigma}(\frac{3}{2})\right] \end{pmatrix}. \quad (2.5)$$

The connection between the BB isospin states and the SU(3)-irreps is given in Table I, and in the figures of Appendix A the NN, YN, and YY content is given for the irreps {8}, {27}, {10*}, {10} and {1}.

The momentum space and configuration space potentials for the ESC16-model have been described in papers I and II for baryon-baryon in general. Therefore, they apply also to hyperon-hyperon and we can refer for that part of the potential to these papers. Also in the ESC-model, the potentials are of such a form that they are exactly equivalent in both momentum space and configuration space. The treatment of the mass differences among the baryons

are handled exactly similar as is done in [31, 32]. Also, exchange potentials related to strange meson exchange K, K^* etc. , can be found in these references.

The baryon mass differences in the intermediate states for TME- and MPE- potentials have been neglected for *YN and YY* scattering. This, although possible in principle, becomes rather laborious and is not expected to change the characteristics of the baryon-baryon potentials.

TABLE I: SU(3) content of the different interaction channels. S is the total strangeness and I is the isospin. The upper half refers to the space-spin symmetric states $^3S_1$, $^1P_1$, ^3D, ..., while the lower half refers to the space-spin antisymmetric states $^1S_0$, ^3P, $^1D_2$, ...

Space-spin symmetric			
S	I	Channels	SU(3)-irreps
0	0	NN	$\{10^*\}$
–1	1/2	$\Lambda N, \Sigma N$	$\{10^*\}, \{8\}_a$
	3/2	ΣN	$\{10\}$
–2	0	ΞN	$\{8\}_a$
	1	$\Xi N, \Sigma\Sigma$	$\{10\}, \{10^*\}, \{8\}_a$
		$\Sigma\Lambda$	$\{10\}, \{10^*\}$
–3	1/2	$\Xi\Lambda, \Xi\Sigma$	$\{10\}, \{8\}_a$
	3/2	$\Xi\Sigma$	$\{10^*\}$
–4	0	$\Xi\Xi$	$\{10\}$
Space-spin antisymmetric			
S	I	Channels	SU(3)-irreps
0	1	NN	$\{27\}$
–1	1/2	$\Lambda N, \Sigma N$	$\{27\}, \{8\}_s$
	3/2	ΣN	$\{27\}$
–2	0	$\Lambda\Lambda, \Xi N, \Sigma\Sigma$	$\{27\}, \{8\}_s, \{1\}$
	1	$\Xi N, \Sigma\Lambda$	$\{27\}, \{8\}_s$
	2	$\Sigma\Sigma$	$\{27\}$
–3	1/2	$\Xi\Lambda, \Xi\Sigma$	$\{27\}, \{8\}_s$
	3/2	$\Xi\Sigma$	$\{27\}$
–4	1	$\Xi\Xi$	$\{27\}$

B. SU(3) Symmetry and R-conjugation

The SU(3)-invariant interaction Hamiltonian for the baryon-baryon (BB) pseudoscalar (P) meson interaction reads [34]

$$\begin{aligned}\mathcal{H}_I \;=\; & g_{P,8}\sqrt{2}\{\alpha_P\,[\bar{B}BP]_F + (1-\alpha_P)\,[\bar{B}BP]_D\} \\ & + g_{P,1}\,[\bar{B}BP]_S\,. \end{aligned} \tag{2.6}$$

Here, the baryons are the members of the $J^P = \frac{1}{2}^+$ baryon octet

$$B = \begin{pmatrix} \frac{\Sigma^0}{\sqrt{2}} + \frac{\Lambda}{\sqrt{6}} & \Sigma^+ & p \\ \Sigma^- & -\frac{\Sigma^0}{\sqrt{2}} + \frac{\Lambda}{\sqrt{6}} & n \\ -\Xi^- & \Xi^0 & -\frac{2\Lambda}{\sqrt{6}} \end{pmatrix}. \tag{2.7}$$

The meson nonet 3×3 matrix P can be written as

$$P = P_{\{1\}} + P_{\{8\}}, \tag{2.8}$$

where the singlet 3×3 matrix $P_{\{1\}}$ has the elements $\eta_0/\sqrt{3}\delta^\alpha_\beta$, and the octet matrix $P_{\{8\}}$ is given by

$$P_{\{8\}} = \begin{pmatrix} \frac{\pi^0}{\sqrt{2}} + \frac{\eta_8}{\sqrt{6}} & \pi^+ & K^+ \\ \pi^- & -\frac{\pi^0}{\sqrt{2}} + \frac{\eta_8}{\sqrt{6}} & K^0 \\ K^- & \overline{K^0} & -\frac{2\eta_8}{\sqrt{6}} \end{pmatrix}. \tag{2.9}$$

Similarly the interaction with the vector $J^{PC} = 1^{--}$, scalar $J^{PC} = 0^{++}$, axial-vectors $J^{PC} = 1^{++}$ and $J^{PC} = 1^{+-}$ mesons. With the SU(2) isosinglet Λ, isodoublets

$$\begin{aligned} N &= \begin{pmatrix} p \\ n \end{pmatrix}, \quad \Xi = \begin{pmatrix} \Xi^0 \\ \Xi^- \end{pmatrix}, \quad \text{and} \\ K &= \begin{pmatrix} K^+ \\ K^0 \end{pmatrix}, \quad K_c = \begin{pmatrix} \overline{K^0} \\ -K^- \end{pmatrix}, \end{aligned} \tag{2.10}$$

and isovectors $(\Sigma^+, \Sigma^0, \Sigma^-)$ and (π^+, π^0, π^-), the SU(3) invariant interaction Hamiltonian (2.6) can be written in the isospin basis, see *e.g.* [34] and [3] formula (2.9). All coupling constants can be expressed in terms of only four parameters. The explicit expressions can be found in Refs. [31, 34]. For example, in the case of the pseudoscalar mesons the parameters are (i) the octet coupling $g_{NN\pi}$, the F/(F+D)-ratio α_P, the singlet coupling g_{η_0}, and the $\eta_8 - \eta_0$ mixing angle θ_P. In Table II B the relation between the potentials on the isospin-basis is given, see (2.4)-(2.5), and the SU(3)-irreps. Here $V_{\Xi\Xi} = V_{\Xi\Xi,\Xi\Xi}, V_{\Lambda\Lambda} = V_{\Lambda\Xi,\Lambda\Xi}$ etc.

In paper III we have introduced as an extension of the ESC16 model the ESC16* models A and B with additional SU(3)-symmetric central and spin-spin gaussian-contact BB s-channel potentials

$$W_{\mu,c}(r) = A_\mu f_W(r),\ W_{\mu,\sigma}(r) = B_\mu f_W(r) \boldsymbol{\sigma}_1 \cdot \boldsymbol{\sigma}_2,$$

where $f_W(r) = m_W \exp(-m_W^2 r^2)$, $m_W = 300$ MeV. The s-channel coefficients A_μ, B_μ for ESC16*(A) are derived from Tables XVIII and XIX in paper III, and given in Table III. Here,

TABLE II: SU(3)-contents of the various potentials on the isospin basis.

Space-spin antisymmetric states ${}^1S_0,\ {}^3P,\ {}^1D_2, ...$		
$\Xi\Xi \to \Xi\Xi$	$Y=-2, I=1$	$V_{\Xi\Xi}(I=1) = V_{27}$
$\Lambda\Xi \to \Lambda\Xi$		$V_{\Lambda\Lambda}\left(I=\frac{1}{2}\right) = \left(9V_{27}+V_{8_s}\right)/10$
$\Lambda\Xi \to \Sigma\Xi$	$Y=-1, I=\frac{1}{2}$	$V_{\Sigma\Lambda}\left(I=\frac{1}{2}\right) = \left(-3V_{27}+3V_{8_s}\right)/10$
$\Sigma\Xi \to \Sigma\Xi$		$V_{\Sigma\Sigma}\left(I=\frac{1}{2}\right) = \left(V_{27}+9V_{8_s}\right)/10$
$\Sigma\Xi \to \Sigma\Xi$	$Y=-1, I=\frac{3}{2}$	$V_{\Sigma\Sigma}\left(I=\frac{3}{2}\right) = V_{27}$
Space-spin symmetric states ${}^3S_1,\ {}^1P_1,\ {}^3D, ...$		
$\Xi\Xi \to \Xi\Xi$	$Y=-2, I=0$	$V_{\Xi\Xi}(I=0) = V_{10}$
$\Lambda\Xi \to \Lambda\Xi$		$V_{\Lambda\Lambda}\left(I=\frac{1}{2}\right) = \left(V_{10}+V_{8_a}\right)/2$
$\Lambda\Xi \to \Sigma\Xi$	$Y=-1, I=\frac{1}{2}$	$V_{\Sigma\Lambda}\left(I=\frac{1}{2}\right) = \left(V_{10}-V_{8_a}\right)/2$
$\Sigma\Xi \to \Sigma\Xi$		$V_{\Sigma\Sigma}\left(I=\frac{1}{2}\right) = \left(V_{10}+V_{8_a}\right)/2$
$\Sigma\Xi \to \Sigma\Xi$	$Y=-1, I=\frac{3}{2}$	$V_{\Sigma\Sigma}\left(I=\frac{3}{2}\right) = V_{10^\star}$

TABLE III: ESC16*(A): Coupling constants SU(3)-symmetric gaussian potentials.

$\{\mu\}$	$\{27\}$	$\{8_s\}$	$\{1\}$	$\{8_a\}$	$\{10^*\}$	$\{10\}$
$A_{\{\mu\}}$	–0.109	–0.219	–1.568	–3.322	–0.635	–0.635
$B_{\{\mu\}}$	0.156	–0.356	0.459	3.594	0.123	0.123

we have chosen to exhibit the s-channel contact-potentials rather than the t,u-channel ones in paper III. The largest contact-potentials occur in the $\{8_a\}$ and $\{1\}$ irreps. The s-channel coefficients for model ESC16*(B) with R-symmetry [35] for the gaussian contact BB potentials are given in Table IV.

For model ESC16*(A) the entries for the irreps $\{10\}$ and $\{10^*\}$ in Table III are the same. The reason is that we neglect the $\{8_s\} \leftrightarrow \{8_a\}$ transitions in the contact potentials. These lead to spin singlet-triplet transitions ${}^1P_1 \leftrightarrow {}^3P_1$ etc., which are small and do not occur in s-waves. So, de facto the contact potentials have R-symmetry.

TABLE IV: ESC16*(B): Coupling constants SU(3)-symmetric gaussian potentials.

$\{\mu\}$	$\{27\}$	$\{8_s\}$	$\{1\}$	$\{8_a\}$	$\{10^*\}$	$\{10\}$
$A_{\{\mu\}}$	–0.118	0.071	–0.874	–3.003	–1.635	–1.635
$B_{\{\mu\}}$	0.261	–0.851	0.084	3.268	–0.302	–0.302

To compare the SU(3)-structure for the BB-states Gell-Mann's R-conjugation [35, 36] is

useful. R-conjugation is the inversion operation on the baryon and pseudo-scalar octet states

$$p \leftrightarrow \Xi^-, \;\; n \leftrightarrow \Xi^0, \;\; \Lambda \leftrightarrow \Lambda, \;\; \Sigma^0 \leftrightarrow \Sigma^0, \tag{2.11}$$

$$K^+ \leftrightarrow K^-, \;\; K^0 \leftrightarrow \bar{K}^0, \;\; \eta \leftrightarrow \eta, \;\; \pi^0 \leftrightarrow \pi^0. \tag{2.12}$$

For the BB-states one has

$$\begin{aligned} R\psi_{27}(Y,I,I_3) &= \psi_{27}(-Y,I,-I_3)\,, \\ R\psi_{10}(Y,I,I_3) &= \psi_{10^\star}(-Y,I,-I_3)\,, \\ R\psi_{8_s}(Y,I,I_3) &= \psi_{8_s}(-Y,I,-I_3)\,, \\ R\psi_{8_a}(Y,I,I_3) &= -\psi_{8_a}(-Y,I,-I_3)\,, \\ R\psi_{1}(Y,I,I_3) &= \psi_{1}(-Y,I,-I_3). \end{aligned} \tag{2.13}$$

Therefore, in comparing the SU(3)-structure of the $(\Lambda N, \Sigma N)$-potentials with the $(\Lambda\Xi, \Sigma\Xi)$-potentials the irreps $\{10\}$ and $\{10^\star\}$ are interchanged. Similarly, for the NN-potentials and the $\Xi\Xi$-potentials. The entries of Table II B, apart from using SU(3) Clebsch-Gordan coefficients, can be derived from Table I in Ref. [2] using R-conjugation.

The R-conjugation is not an SU(3)-transformation, and also it is not a symmetry of the strong-interactions. The latter would mean no $\{8_s\} \leftrightarrow \{8_a\}$-transitions, because $\langle\{8_a\}|V|\{8_s\}\rangle = \langle\{8_a\}|R^{-1}VR|\{8_s\}\rangle = -\langle\{8_a\}|V|\{8_s\}\rangle = 0$. This would imply that the transitions ${}^1P_1 \leftrightarrow {}^3P_1$ are forbidden, and so no anti-symmetric spin-orbit forces. However, for the vector- and axial-vector exchange with different F/(F+D) ratios for the direct and derivative couplings the antisymmetric spin-orbit potentials are non-zero, while having SU(3) symmetry. The extra restriction from R-conjugation symmetry w.r.t. SU(3) is that $V_{\{10\}} = V_{\{10^*\}}$. Then, the central-, spin-spin-, tensor-, spin-orbit-, and quadratic spin-orbit potential have R-symmetry for exact SU(3) symmetry. In the ESC models the $V_{10} \approx V_{10^*}$, see [3], and the singlet-triplet transitions are small. So, we conclude that R-conjugation is an approximate symmetry in the ESC models, and is broken "kinematically" exactly similar to SU(3).

C. Solving the multi-channel Schrödinger equation

The method of evaluation of the ESC16 models for the S=-3,-4 channels follows closely that for the S=0,-1,-2 channels. For details see paper III [3], sections II and III. The main features are: (i) The multi-channel Schrödinger equation is solved for the physical particle channels. The S=-3,-4 BB-channels can be classified according to their total charge Q; these are given in (2.1). (ii) Average baryon and meson masses are used in the potentials, *i.e.* isospin is treated as a good quantum number. The only breaking of isospin symmetry occurs via the inclusion of the Coulomb interaction. (iii) The isospin matrix elements for the various OBE potentials are given in Table V, where we use the pseudoscalar mesons as a specific example. The flavor-exchange operator P_f is $+1$ for a flavor symmetric and -1 for a flavor anti-symmetric states. Since two-baryons states are totally anti-symmetric $P_f = -P_x P_\sigma$. Therefore, the exchange operator P_f has the value $P_f = +1$ for even-L singlet and odd-L triplet partial waves, and $P_f = -1$ for odd-L singlet and even-L triplet partial waves. For total strangeness $S = -3$, the final-state interchanged diagram only occurs when the exchanged meson carries strangeness (K, K^*, κ, K^{**}). (iv) For a proper derivation of the exchange operator P_f and the exchange forces, see Ref. [3] section III.

TABLE V: Isospin factors for the various meson exchanges in the different channels with total strangeness and isospin. P_f is the flavor-exchange operator. Non-existing channels are marked by a long-dash.

$S=-3$	$I=1/2$	$I=3/2$
$(\Lambda\Xi\|\eta,\eta'\|\Lambda\Xi)$	1	—
$(\Sigma\Xi\|\eta,\eta'\|\Sigma\Xi)$	1	1
$(\Sigma\Xi\|\pi\|\Sigma\Xi)$	-2	1
$(\Sigma\Xi\|\pi\|\Lambda\Xi)$	$\sqrt{3}$	—
$(\Lambda\Xi\|K\|\Xi\Lambda)$	P_f	—
$(\Sigma\Xi\|K\|\Xi\Sigma)$	$-P_f$	$2P_f$
$(\Lambda\Xi\|K\|\Xi\Sigma)$	$P_f\sqrt{3}$	—
$S=-4$	$I=0$	$I=1$
$(\Xi\Xi\|\eta,\eta'\|\Xi\Xi)$	$\frac{1}{2}(1-P_f)$	$\frac{1}{2}(1+P_f)$
$(\Xi\Xi\|\pi\|\Xi\Xi)$	$-\frac{3}{2}(1-P_f)$	$\frac{1}{2}(1+P_f)$

III. MULTI-CHANNEL THRESHOLDS S=-3 CHANNELS

As seen from (2.1) the $S=-3$ two-baryon channels consist of two separate coupled-channel systems separated by the charge. The thresholds are due to the baryon mass differences. The used baryon masses are the same as in [1–3], and are given in Table VI. The

TABLE VI: Baryon masses in MeV/c^2.

Baryon		Mass
Nucleon	p	938.2796
	n	939.5731
Hyperon	Λ	1115.60
	Σ^+	1189.37
	Σ^0	1192.46
	Σ^-	1197.436
Cascade	Ξ^0	1314.90
	Ξ^-	1321.32

laboratory momenta, starting from the baryons at the lowest threshold, are shown in Fig. 1. Taking the charge dependence of the masses into account gives a splitting of the thresholds, *e.g.*:
For $(\Lambda\Xi^-, \Sigma^-\Xi^0, \Sigma^0\Xi^-)$:

$$\begin{aligned} p_\Lambda^{th}(\Lambda\Xi^- \to \Sigma^-\Xi^0) &= 578.9 \text{ MeV/c}, \\ p_\Lambda^{th}(\Lambda\Xi^- \to \Sigma^0\Xi^-) &= 584.8 \text{ MeV/c}. \end{aligned} \tag{3.1}$$

For $(\Lambda\Xi^0, \Sigma^0\Xi^0, \Sigma^+\Xi^-)$:

$$\begin{aligned} p_\Lambda^{th}(\Lambda\Xi^0 \to \Sigma^0\Xi^0) &= 572.2 \text{ MeV/c}, \\ p_\Lambda^{th}(\Lambda\Xi^0 \to \Sigma^+\Xi^-) &= 585.5 \text{ MeV/c}. \end{aligned} \tag{3.2}$$

The meson masses are the same as in [1–3], as well as the cut-off masses. The threshold differences lead to effective masses for the meson with non-zero strangeness, see [3, 4, 37] for details and references. For S=-3 channels these masses are for the pseudoscalar meson $m_K = 453.4$ MeV, and the vector meson $m_{K^*} = 869.1$ MeV, These effects are not included for the scalar and axial mesons.

A further subdivision is according to the total isospin. The different thresholds have been discussed in detail in [4], and we show them here in Fig. 1 for the purpose of general orientation. Their presence turns the Lippmann-Schwinger and Schrödinger equation into a coupled-channel matrix equation, where the different channels open up at different energies. In general one has a combination of 'open' and 'closed' channels. For a discussion of the solution of such a mixed system, we refer to [37].

IV. ESC-MODEL PARAMETERS

A complete set of meson coupling constants for ESC16 and ESC16* are given in Appendix B, Tables VII, and VIII, respectively. The corresponding meson-pair couplings are given in Appendix C, Tables IX, and X, respectively.

For other model parameters as gaussian cut-off's, meson mixing angles, etc. see Ref.'s [1–3].

V. RESULTS

The main purpose of this paper is to present the properties of the ESC16, and ESC16* potentials for the S=-3,-4 sectors. We found that the results for S=-3,-4 for the different models are not significantly different. We will show the detailed results for ESC16, which are sufficient to represent the possible kind of results.

In the following we will present the model predictions for scattering lengths, bound states, and cross sections.

A. Effective-range parameters

The (multi-channel) effective-range expansion, see [33], reads

$$\begin{aligned} & p^{L+1/2}(\bar{K}^J)^{-1}p^{L+1/2} \\ & \quad -A^{-1} + \frac{1}{2}(p^2 - p_0^2)^{1/2}\, R\, (p^2 - p_0^2)^{1/2}, \end{aligned}$$

where $\bar{K}^J$ is the mutilated K^J matrix with the $^3D_1$ channels being cut out, A^{-1} is the inverse scattering-length matrix, R the effective-range matrix, $p^{L+1/2}$ and $(p^2 - p_0^2)^{1/2}$ are the diagonal matrices with elements $p_i^{L+1/2}$ and $(p_i^2 - p_{0i}^2)^{1/2}$. Here, p_{0i} denotes the momentum at the $\Sigma\Xi^0$-threshold, see below.

Next, we give the low-energy parameters, *i.e.* scattering-lengths and effective-ranges, for the following models:

B. S=-4 Results

The following S=-4 low-energy parameters of ESC16 are obtained, where the C denotes Coulomb included

$$\begin{aligned} a^C_{\Xi\Xi}(^1S_0) &= -1.81\,[fm],\ r^C_{\Xi\Xi}(^1S_0) = 3.89\,[fm], \\ a_{\Xi\Xi}(^1S_0) &= -1.90\,[fm],\ r_{\Xi\Xi}(^1S_0) = 4.28\,[fm], \\ a_{\Xi\Xi}(^3S_1) &= +0.52\,[fm],\ r_{\Xi\Xi}(^3S_1) = 2.74\,[fm]. \end{aligned}$$

For ESC16*(A):

$$\begin{aligned} a_{\Xi\Xi}(^1S_0) &= -1.69\,[fm],\ r_{\Xi\Xi}(^1S_0) = 4.71\,[fm], \\ a_{\Xi\Xi}(^3S_1) &= +0.48\,[fm],\ r_{\Xi\Xi}(^3S_1) = 3.41\,[fm]. \end{aligned}$$

For ESC16*(B):

$$\begin{aligned} a_{\Xi\Xi}(^1S_0) &= -1.86\,[fm],\ r_{\Xi\Xi}(^1S_0) = 4.45\,[fm], \\ a_{\Xi\Xi}(^3S_1) &= +0.49\,[fm],\ r_{\Xi\Xi}(^3S_1) = 3.16\,[fm]. \end{aligned}$$

C. S=-3,I=3/2 Results

For ESC16:

$$\begin{aligned} a_{\Sigma\Xi^0}(^1S_0) &= -1.71\,[fm],\ r_{\Sigma\Xi^0}(^1S_0) = 3.71\,[fm], \\ a_{\Sigma\Xi^0}(^3S_1) &= -0.85\,[fm],\ r_{\Sigma\Xi^0}(^3S_1) = 8.02\,[fm]. \end{aligned}$$

For ESC16*(A):

$$\begin{aligned} a_{\Sigma\Xi}(^1S_0) &= -1.41\,[fm],\ r_{\Sigma\Xi}(^1S_0) = 4.29\,[fm], \\ a_{\Sigma\Xi}(^3S_1) &= -1.31\,[fm],\ r_{\Sigma\Xi}(^3S_1) = 5.47\,[fm]. \end{aligned}$$

For ESC16*(B):

$$\begin{aligned} a_{\Sigma\Xi}(^1S_0) &= -1.64\,[fm],\ r_{\Sigma\Xi}(^1S_0) = 4.00\,[fm], \\ a_{\Sigma\Xi}(^3S_1) &= -1.90\,[fm],\ r_{\Sigma\Xi}(^3S_1) = 4.20\,[fm]. \end{aligned}$$

D. S=-3,I=1/2 Results

For ESC16:

$$\begin{aligned} a_{\Lambda\Xi^0}(^1S_0) &= -0.56\,[fm],\ r_{\Lambda\Xi^0}(^1S_0) = 8.32\,[fm], \\ a_{\Lambda\Xi^0}(^3S_1) &= +0.40\,[fm],\ r_{\Lambda\Xi^0}(^3S_1) = 2.52\,[fm]. \end{aligned}$$

Around the $\Sigma\Xi^0$-threshold for I=1/2 states

$$\begin{aligned}
\Sigma\Xi^0(^1S_0) \;:\; A^{-1} &= \begin{pmatrix} 31.537 & -29.454 \\ -29.454 & 34.928 \end{pmatrix}, \\
R &= \begin{pmatrix} 89.479 & 19.524 \\ 19.524 & -160.211 \end{pmatrix}, \\
\Sigma\Xi^0(^3S_1) \;:\; A^{-1} &= \begin{pmatrix} 1.708 & 2.377 & 0.662 \\ 2.377 & 62.133 & -16.828 \\ 0.662 & -16.828 & 2.377 \end{pmatrix}, \\
R &= \begin{pmatrix} -0.208 & 13.675 & -3.522 \\ 13.675 & -472.466 & 98.143 \\ -3.522 & 98.143 & -15.637 \end{pmatrix},
\end{aligned}$$

For ESC16*(A):

$$\begin{aligned}
a_{\Lambda\Xi^0}(^1S_0) &= -1.147\,[fm],\; r_{\Lambda\Xi^0}(^1S_0) = 4.849\,[fm], \\
a_{\Lambda\Xi^0}(^3S_1) &= +0.088\,[fm],\; r_{\Lambda\Xi^0}(^3S_1) = 76.227\,[fm].
\end{aligned}$$

Around the $\Sigma\Xi^0$-threshold for I=1/2 states

$$\begin{aligned}
\Sigma\Xi^0(^1S_0) \;:\; A^{-1} &= \begin{pmatrix} 6.641 & 2.230 \\ 2.230 & -1.110 \end{pmatrix}, \\
R &= \begin{pmatrix} -18.459 & 10.465 \\ 10.465 & 2.826 \end{pmatrix}, \\
\Sigma\Xi^0(^3S_1) \;:\; A^{-1} &= \begin{pmatrix} 2.750 & 6.882 & -0.150 \\ 6.882 & -89.577 & 2.952 \\ -0.150 & 2.952 & -0.267 \end{pmatrix}, \\
R &= \begin{pmatrix} -0.410 & 17.883 & -2.294 \\ 17.883 & -312.978 & 45.798 \\ -2.294 & 45.798 & -3.493 \end{pmatrix},
\end{aligned}$$

For ESC16*(B):

$$\begin{aligned}
a_{\Lambda\Xi^0}(^1S_0) &= -1.382\,[fm],\; r_{\Lambda\Xi^0}(^1S_0) = 4.342\,[fm], \\
a_{\Lambda\Xi^0}(^3S_1) &= +0.002\,[fm],\; r_{\Lambda\Xi^0}(^3S_1) = 1.079 * 10^2\,[fm].
\end{aligned}$$

Around the $\Sigma\Xi^0$-threshold for I=1/2 states

$$\Sigma\Xi^0(^1S_0) \;:\; A^{-1} = \begin{pmatrix} 8.826 & 1.680 \\ 1.680 & -0.569 \end{pmatrix},$$
$$R = \begin{pmatrix} -14.077 & 9.210 \\ 9.210 & 2.375 \end{pmatrix},$$
$$\Sigma\Xi^0(^3S_1) \;:\; A^{-1} = \begin{pmatrix} 3.018 & 6.448 & -0.004 \\ 6.448 & -61.994 & 0.131 \\ -0.004 & 0.131 & 0.210 \end{pmatrix},$$
$$R = \begin{pmatrix} 0.648 & 5.124 & -0.729 \\ 5.124 & -232.352 & 34.303 \\ -0.729 & 34.303 & -2.321 \end{pmatrix}.$$

E. Bound states in S waves

The scattering lenghts and effective ranges in both models show no sign of a bound state. In particular this is the case for $\Xi\Xi(^1S_0)$, which shows a weaker attraction than in $pp(^1S_0)$. Similarly for $\Xi\Xi(^3S_1)$. The effective range formula for the pole position of a possible bound state in momentum space is

$$\kappa_\pm = \left(1 \pm \sqrt{1 - 2r/a}\right)/r,\; B_\pm = -\kappa_\pm^2/(2m_{red}),$$

where the momentum is $p_\pm = i\kappa_\pm$. The pole closest to the lowest threshold is given by κ_-, and (usually) κ_+ is outside the region of the approximate validity of the effective-range formula. which for $\Xi\Xi(^1S_0)$ gives $\kappa_- < 0$, meaning an anti-bound state, and κ_+ is too large for the effective range expansion to be valid. In the case of $\Xi\Xi(^3S_1)$ the root is imaginary, and so no bound state. (Apparently there is enough SU(3)- and R-symmetry breaking to prevent a deuteron-like bound state in this channel.) Similar analysis shows that also in the other channels there do not occur bound states.

A discussion of the possible bound-states, using the SU(3) content of the different $S = 0, -1, -2$ channels is given in [31]. In contrast to the NSC97 models, we find no S<0 bound states in the ESC16 models.

F. Partial Wave Phase BKS-Parameters

For the *BB*-channels below the inelastic threshold we use for the parametrization of the amplitudes the standard nuclear-bar phase shifts [38]. The information on the elastic amplitudes above thresholds is most conveniently given using the BKS-phases [39–42]. For uncoupled partial waves, the elastic *BB* S-matrix element is parametrized as

$$S = \eta e^{2i\delta}\,,\;\; \eta = \cos(2\rho)\,. \tag{5.1}$$

For coupled partial waves the elastic *BB*-amplitudes are 2×2-matrices. The BKS S-matrix parametrization reads

$$S = e^{i\delta} e^{i\epsilon} N \, e^{i\epsilon} e^{i\delta} \, , \tag{5.2}$$

where

$$\delta = \begin{pmatrix} \delta_\alpha & 0 \\ 0 & \delta_\beta \end{pmatrix} , \;\; \epsilon = \begin{pmatrix} 0 & \epsilon \\ \epsilon & 0 \end{pmatrix} , \tag{5.3}$$

and N is a real, symmetric matrix parametrize as

$$N = \begin{pmatrix} \eta_{11} & \eta_{12} \\ \eta_{12} & \eta_{22} \end{pmatrix} . \tag{5.4}$$

In Fig. 2 the S=-4 ESC16 nuclear-bar phases for $\Xi^0\Xi^0(^1S_0, I = 1)$ and $\Xi^0\Xi^-(^3S_1, I = 0)$ are shown. Fig. 3 shows the $\Lambda\Xi^0(^1S_0)$ and $\Lambda\Xi^-(^3S_1 - ^3D_1)$ phase parameters. Fig. 4 and Fig. 5 show for ESC16 the $\Sigma^0\Xi^0(I = 1/2)$ BKS phase shift and inelasticity parameters for $^1S_0$ and $^3S_1$ respectively. Similarly, Fig. 6 shows the $\Sigma^+\Xi^0(I = 3/2)$ phase shifts.

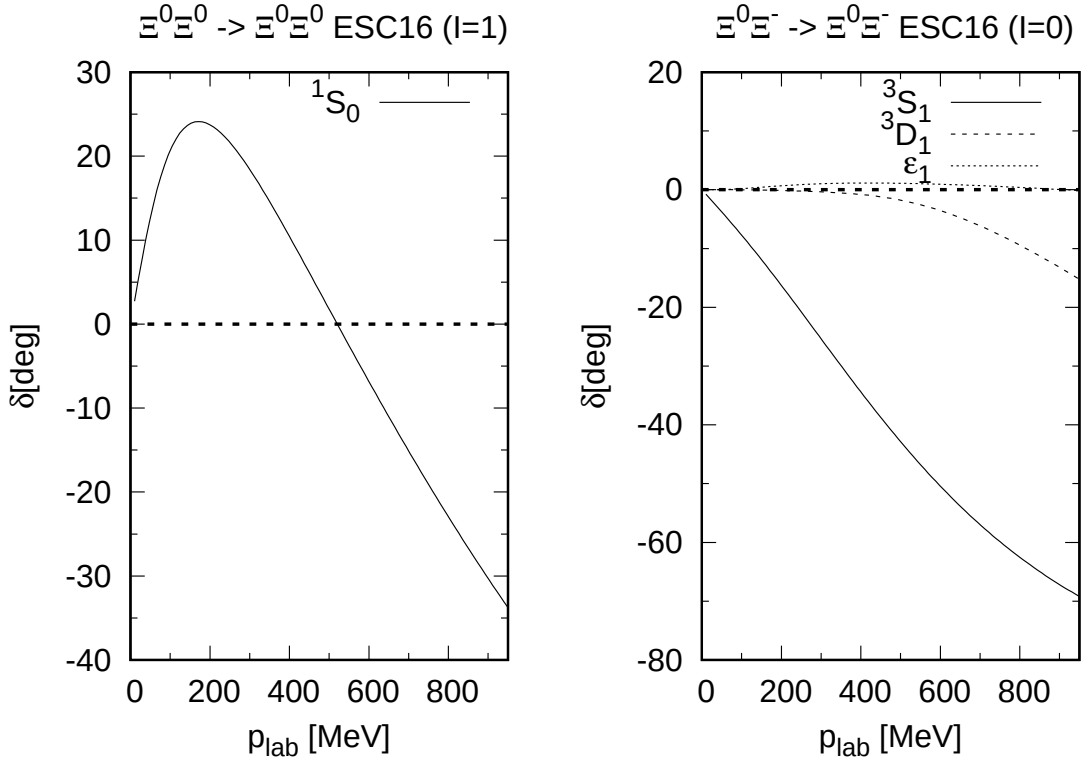

FIG. 2: ESC16 $\Xi^0\Xi^0(^1S_0, I = 1)$- and $\Xi^0\Xi^-(^3S_1, I = 0)$ phases.

The $\Xi^-\Xi^-, \Xi^0\Xi-, \Xi^0\Xi^0$ nuclear-bar phase shifts for I=1 and I=0 as a function of the momentum and energy are given in the tables in Appendix D for ESC16, and in Appendix E for ESC16*(A). Similarly, for the BKS-parameters $\Lambda\Xi^0, \Lambda\Xi(I = 1/2), \Sigma\Xi^0(I = 1/2)$, and $\Sigma^+\Xi^0(I = 3/2)$. the inelasticity parameters ρ and $\eta_{11}, \eta_{12}, \eta_{22}$, which contains the information to construct the $\delta-$, $\epsilon-$, N- and S-matrix.

The $\Xi\Xi(^1S_0, I = 1)$ phase shift is in agreement with LQCD, see Ref. [12] Fig.2. For example at $p_{lab} = 200$ MeV/c, which means $T_{cm} = 3.8$ MeV, ESC16 has $\delta(^1S_0, I = 1) = 23.71$ deg, see

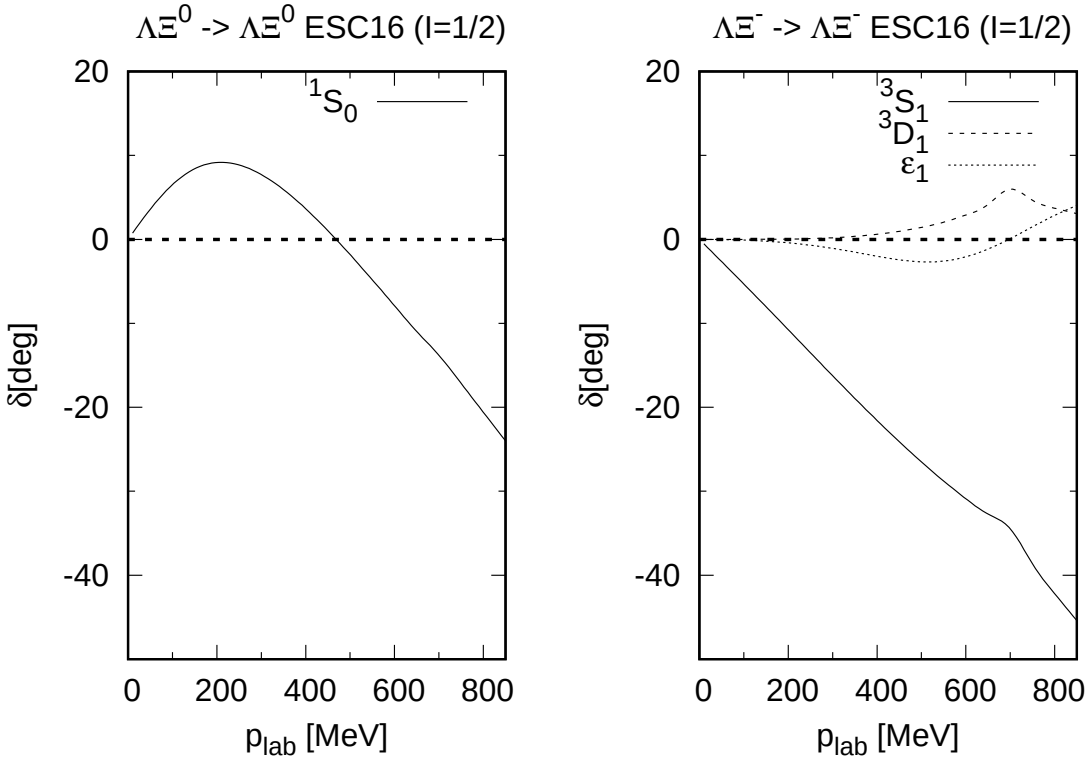

FIG. 3: ESC16 $\Lambda\Xi$ $I = 1/2$ phases.

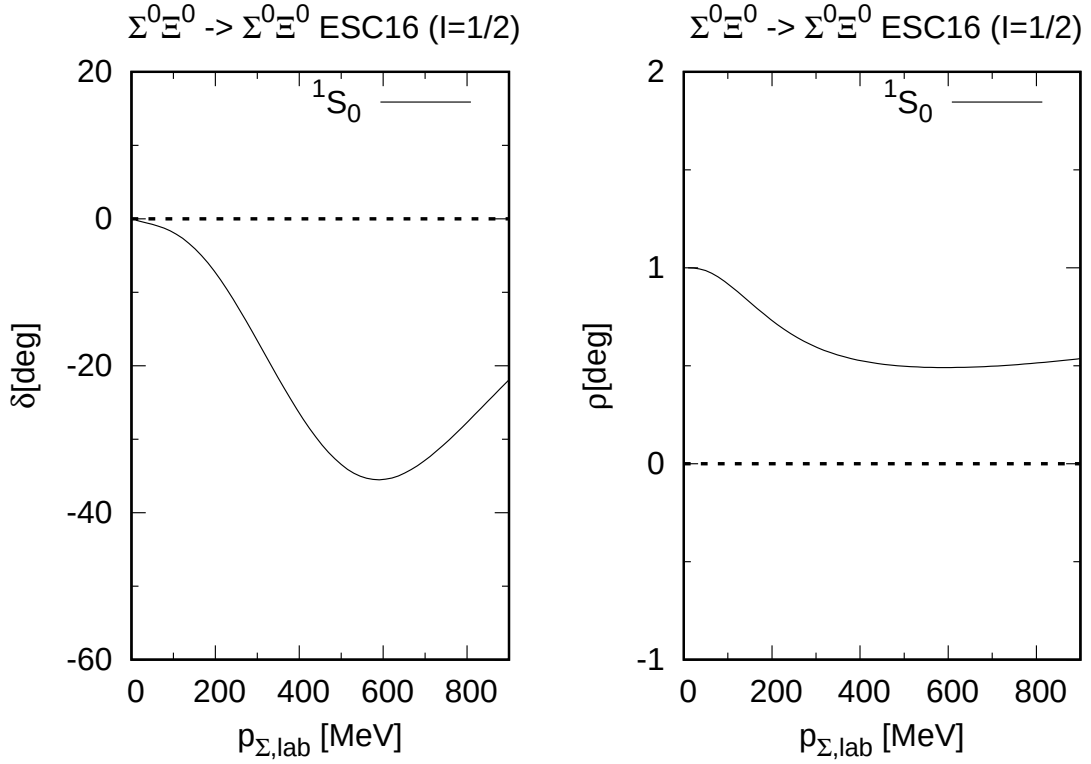

FIG. 4: ESC16 $I = 1/2$ ${}^1S_0(\Sigma^0\Xi^0)$ phases and η-inelasticities.

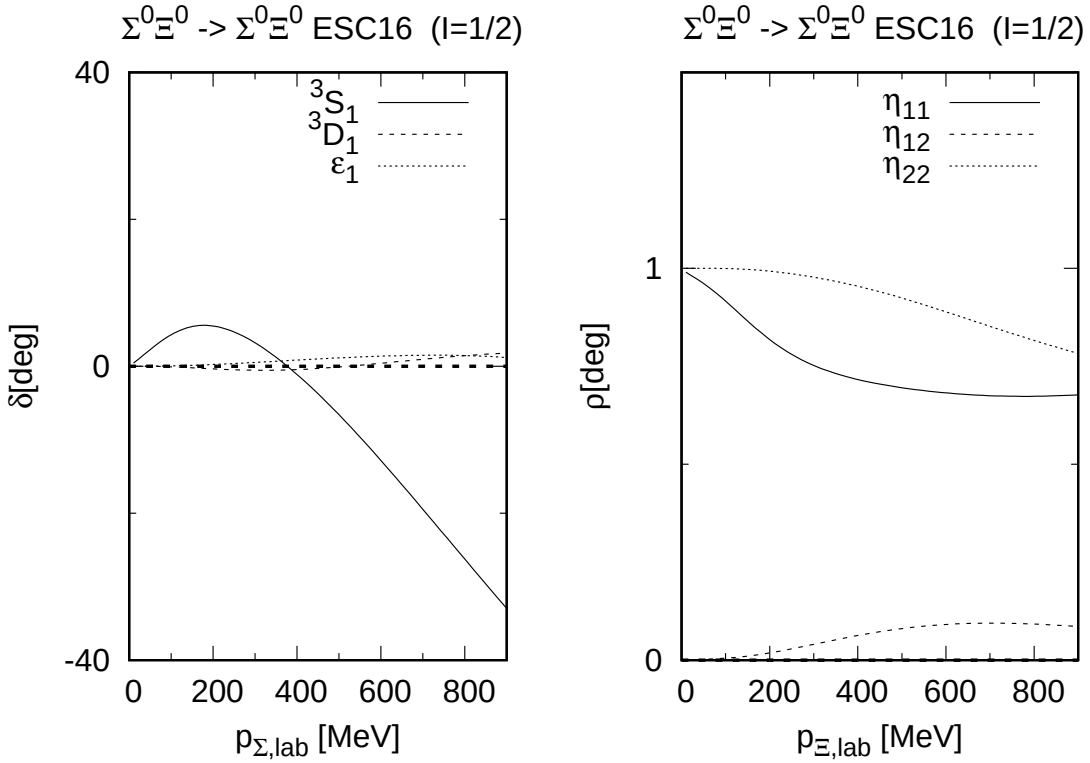

FIG. 5: ESC16 $I = 1/2$ ${}^3C_1(\Sigma^0\Xi^0)$-phases and η-inelasticities.

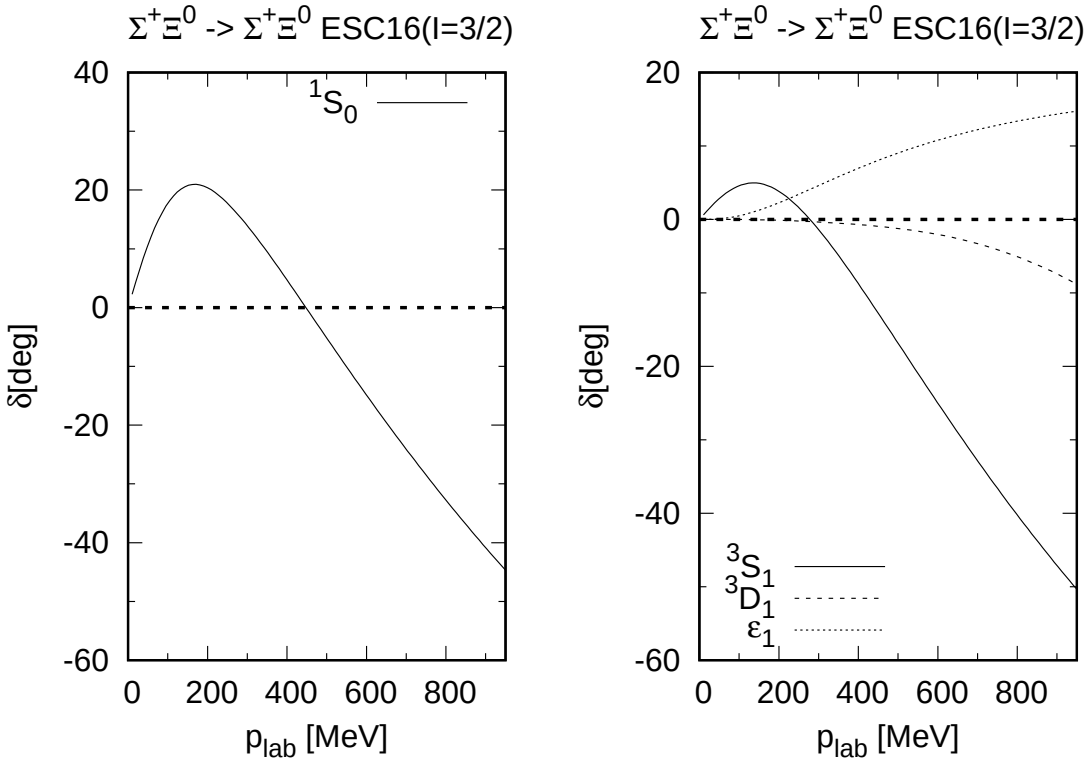

FIG. 6: ESC16 $I = 3/2$ $\Sigma^+\Xi^0$-phases.

Table XI, and ESC16$^\star(A)$ has $\delta(^1S_0, I = 1) = 21.45$ deg, which both match with the LQCD result.
Notice that the $\Xi\Xi(^3S_1, I = 0)$-phase shows repulsion, except for very low energies. This means that the the potential has a weak long range attractive tail from one-pion-exchange. Qualitative this also agrees with the LQCD result.

VI. DISCUSSION AND SUMMARY

An important result is that in the ESC16 models there is no bound state in the $\Xi^0\Xi^0(I = 1,^1 S_0)$-channel, which is in the SU(3)-irrep {27}. Since $pp(^1S_0), nn(^1S_0)$ are in the same irrep and quite attractive it might be expected naively that because of the larger Ξ-mass a bound state might occur. Similarly, in the past sometimes it was speculated that a bound state could appear in Σ^+p. Apparently the breaking of SU(3) symmetry, due to using the physical meson and baryon masses, prevents such bound states.

It is seen from Fig. 2 and Table XII that the $\Xi^0\Xi^0(^1S_0)$ indicate an attractive interaction but this is weaker than in the case of *e.g.* Σ^+p. Also the preliminary data of STAR [14] indicate that the $\Xi\Xi$ interaction in the $^1S_0$ is much weaker than in pp.

In order to illustrate the basic properties of the potentials for S=-3,-4 we have presented results for scattering lengths and phaseshifts in the tables. From these the differential and total cross sections can be calculated easily.

The results for the S=-3,-4 channels of ESC16 and ESC16*(A,B) are qualitatively similar. From Table I it is seen that the same SU(3)-irreps occur in these channels as for S=0,-1, where experimental data determine the interactions to a great extent.

Summarizing, the ESC16 and ESC16*(A,B) provide an SU(3)-based unified realistic description of all BB-interactions, using single (OBE) and double (TME,MPE) meson-exchange potentials with gaussian form factors. Here, the baryons are the SU(3) octet ground-states with $J^P = 1/2^+$. The baryon-meson coupling constants can be systematically related to the quark-antiquark pair creation process with $^3P_0$ dominance. Using (heavy) meson dominance this can be extended to the baryon-meson-pair couplings as well. The ESC-potentials have been applied to calculate the properties of nuclei, hypernuclei, including double-Λ and more exotic YY-hypernuclei. Also, the interactions can be explored to study multiply-strange systems, and strange nuclear matter.

Application of the ESC interactions to the study of all $\{8\} \otimes \{8\}$ two-baryon correlations measured in heavy-ion collission experiments is a future project, with the prospect of further insight into the low and intermediate energy baryon-baryon interactions.

Appendix A: SU(3)-irreps and Baryon-baryon Isospin-states

The BB-irreps are diplayed in Fig. 7 and Fig. 8 showing the two-baryon content, and the hypercharge Y=N+S of the SU(2)-isospin multiplets.

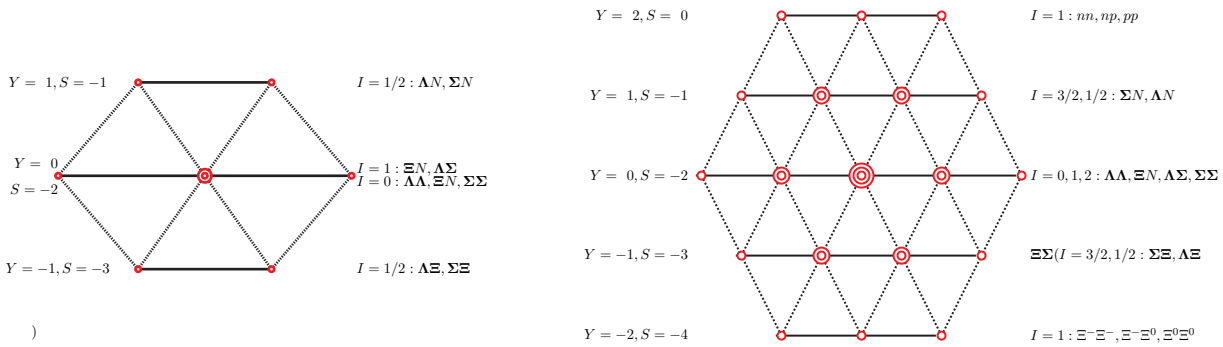

FIG. 7: Baryon-Baryon {8}- and {27}-states.

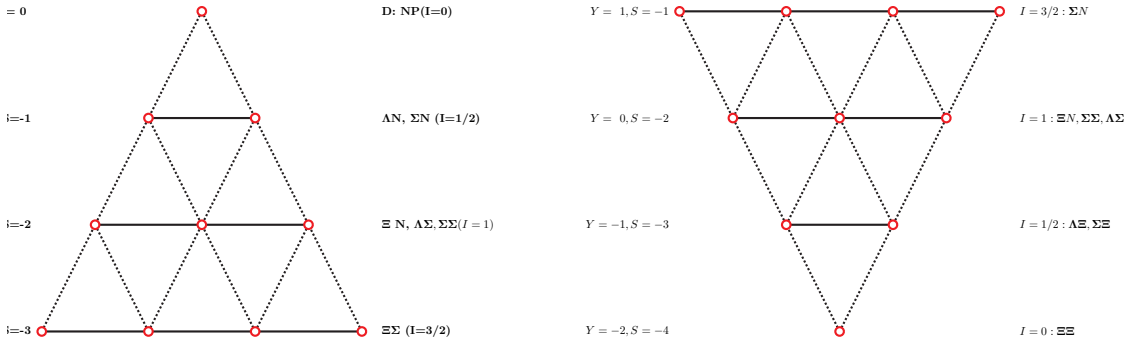

FIG. 8: Baryon-baryon antidecuplet {10*}- and {10}-states.

Appendix B: Meson coupling constants

In Table VII and Table VIII the rationalized NNM, YYM and YNM OBE-couplings are given for models ESC16 and ESC16* respectively. This for pseudoscalar, vector, scalar and axial-vector mesons.

Appendix C: Meson-pair coupling constants

In Table IX and Table X the rationalized NNM_p, YYM_p and YNM_p couplings are given for models ESC16 and ESC16* respectively. This for scalar, vector and axial-vector meson-pairs M_p.

TABLE VII: Coupling constants for model ESC16, divided by $\sqrt{4\pi}$. M refers to the meson. The coupling constants are listed in the order pseudoscalar, vector (g and f), axial vector A (g and f), scalar, axial vector B, and diffractive.

	M	NNM	$\Sigma\Sigma M$	$\Sigma\Lambda M$	$\Xi\Xi M$	M	ΛNM	$\Lambda\Xi M$	ΣNM	$\Sigma\Xi M$
f	π	0.2684	0.1955	0.1968	−0.0725	K	−0.2681	0.0713	0.0725	−0.2684
g	ρ	0.5793	1.1586	0.0000	0.5793	K^*	−1.0034	1.0034	−0.5793	−0.5793
f		3.7791	3.5185	2.3323	−0.2606		−4.2132	1.8810	0.2606	−3.7791
g	a_1	−0.8172	−0.6260	−0.5822	0.1912	K_{1A}	0.8333	−0.2511	−0.1912	0.8172
f		−1.6521	−1.2656	−1.1770	0.3865		1.6846	−0.5076	−0.3865	1.6521
g	a_0	0.5393	1.0786	0.0000	0.5393	κ	−0.9341	0.9341	−0.5393	−0.5393
f	b_1	−2.2598	−1.8078	−1.5656	0.4520	K_{1B}	2.3484	−0.7828	−0.4520	2.2598
	M	NNM	$\Lambda\Lambda M$	$\Sigma\Sigma M$	$\Xi\Xi M$	M	NNM	$\Lambda\Lambda M$	$\Sigma\Sigma M$	$\Xi\Xi M$
f	η	0.1368	−0.1259	0.2599	−0.1958	η'	0.3181	0.3711	0.2933	0.3852
g	ω	3.1148	2.4820	2.4820	1.8492	ϕ	−1.2384	−2.0171	−2.0171	−2.7958
f		−0.5710	−3.2282	−0.2863	−4.4144		2.8878	−0.3819	3.2380	−1.8416
g	f_1'	−0.7596	−0.1213	−1.0133	0.0710	f_1	0.5147	1.0503	0.3019	1.2117
f		−4.4179	−3.1274	−4.9307	−2.7386		4.4754	5.5582	4.0450	5.8844
g	ε	2.9773	2.3284	2.3284	1.6795	f_0	−1.5766	−2.2485	−2.2485	−2.9205
f	h_1'	−1.2386	0.1171	−1.6905	0.5690	h_1	−0.0830	1.8346	−0.7222	2.4738
g	P	2.7191	2.7191	2,7191	2.7197					
g	O	4.1637	4.1637	4.1637	4.1637					
f		−3.8859	−3.8859	−3.8859	−3.8859					

Appendix D: ESC16 BKS-phase parameters

The ESC16 $\Xi^-\Xi^-$ and $\Xi^-\Xi^0$ nuclear-bar phase shifts as a function of energy are given in Tables XII. The $\Lambda\Xi$ BKS phase shifts and inelasticities are given in Table XIII and Table XIV respectively. Table XV shows the $\Sigma^0\Xi^0$ phase parameters, and Table XVI the I=3/2 $\Sigma^+\Xi^0$ phases. Notice that the $^3S_1$-phase shows repulsion, except for very low energies. This means that the the potential has a weak long range attractive tail.

Appendix E: ESC16*(A) BKS-phase parameters

The ESC16*(A) $\Xi^0\Xi^0$ and $\Xi^-\Xi^0$ nuclear-bar phase shifts as a function of energy are given in Tables XVII. The $\Lambda\Xi$ BKS phase shifts and inelasticities are given in Table XVIII and Table XIX respectively. Table XX shows the $\Sigma^0\Xi^0$ phase parameters, and Table XXI the I=3/2 $\Sigma^+\Xi^0$ phases.

TABLE VIII: Coupling constants for model ESC16$^\star(A)$, divided by $\sqrt{4\pi}$. M refers to the meson. The coupling constants are listed in the order pseudoscalar, vector (g and f), axial vector A (g and f), scalar, axial vector B, and diffractive.

	M	NNM	$\Sigma\Sigma M$	$\Sigma\Lambda M$	$\Xi\Xi M$	M	ΛNM	$\Lambda\Xi M$	ΣNM	$\Sigma\Xi M$
f	π	0.2680	0.1978	0.1952	−0.0701	K	−0.2689	0.0737	0.0701	−0.2680
g	ρ	0.5821	1.1641	0.0000	0.5821	K^*	−1.0082	1.0082	−0.5821	−0.5821
f		3.7601	3.8215	2.1355	0.0614		−4.3773	2.2418	−0.0614	−3.7601
g	a_1	−0.8526	−0.6681	−0.5988	0.1845	K_{1A}	0.8780	−0.2792	−0.1845	0.8526
f		−3.1888	−2.4987	−2.2395	0.6902		3.2837	−1.0441	−0.6902	3.1888
g	a_0	0.4905	0.8043	0.1019	0.3139	κ	−0.7575	0.6456	−0.3139	−0.4905
f	b_1	−2.4303	−1.9442	−1.6837	0.4861	K_{1B}	2.5256	−0.8419	−0.4861	2.4303
	M	NNM	$\Lambda\Lambda M$	$\Sigma\Sigma M$	$\Xi\Xi M$	M	NNM	$\Lambda\Lambda M$	$\Sigma\Sigma M$	$\Xi\Xi M$
f	η	0.1394	−0.1243	0.2584	−0.1966	η'	0.3181	0.3712	0.2941	0.3858
g	ω	3.0977	2.4618	2.4618	1.8260	ϕ	−1.2183	−2.0007	−2.0007	−2.7831
f		−0.5473	−3.3080	−0.6144	−4.7218		3.3335	−0.0634	3.2510	−1.8032
g	f_1'	−0.7254	−0.0528	−0.9702	0.1611	f_1	0.4301	0.9945	0.2247	1.1739
f		−4.8976	−2.3822	−5.8134	−1.5824		4.2124	6.3231	3.4440	6.9942
g	ε	3.1268	2.6704	2.7949	2.2762	f_0	−1.5956	−2.1876	−2.0261	−2.6989
f	h_1'	−1.2386	0.2194	−1.7246	0.7054	h_1	−0.1553	1.9069	−0.8428	2.5944
g	P	2.8256	2.8256	2,8256	2.8256					
g	O	4.1637	4.1637	4.1637	4.1637					
f		−3.8859	−3.8859	−3.8859	−3.8859					

TABLE IX: Pair coupling constants for model ESC16, divided by $\sqrt{4\pi}$. $I(M_p)$ refers to the isospin of the pair M_p with quantum-numbers J^{PC}.

Pair	J^{PC}	Type	$I(M_p)$	NNM_p	$\Sigma\Sigma M_p$	$\Sigma\Lambda M_p$	$\Xi\Xi M_p$	$I(M_p)$	ΛNM_p	$\Lambda\Xi M_p$	ΣNM_p	$\Sigma\Xi M_p$
$\pi\eta$	0^{++}	g	1	−0.6881	−1.3763	0.0000	−0.6881	1/2	1.1919	−1.1919	0.6881	0.6881
			0	−1.1919	0.0000	0.0000	1.1919					
$\pi\pi$	1^{--}	g	1	0.2514	0.5028	0.0000	0.2514	1/2	−0.4354	0.4354	−0.2514	−0.2514
			0	0.4354	0.0000	0.0000	−0.4354					
$\pi\pi$	1^{--}	f	1	−1.7729	−1.4183	−1.2283	0.3546	1/2	1.8425	−0.6142	−0.3546	1.7729
			0	−0.6142	1.2283	−1.2283	1.8425					
$\pi\rho$	1^{++}	g	1	5.6913	4.5530	3.9431	−1.1383	1/2	−5.9147	1.9715	1.1383	−5.6913
			0	1.9715	−3.9431	3.9431	−5.9146					
$\pi\sigma$	1^{++}	g	1	−0.3892	−0.3114	−0.2697	0.0778	1/2	0.4045	−0.1348	−0.0778	0.3892
			0	−0.1348	0.2697	−0.2697	0.4045					
$\pi\omega$	1^{+-}	g	1	−0.3281	−0.2624	−0.2273	0.0656	1/2	0.3409	−0.1136	−0.0656	0.3281
			0	−0.1136	0.2273	−0.2273	0.3409					

TABLE X: Pair coupling constants for model ESC16$^\star(A)$, divided by $\sqrt{4\pi}$. $I(M_p)$ refers to the isospin of the pair M_p with quantum-numbers J^{PC}.

Pair	J^{PC}	Type	$I(M_p)$	NNM_p	$\Sigma\Sigma M_p$	$\Sigma\Lambda M_p$	$\Xi\Xi M_p$	$I(M_p)$	ΛNM_p	$\Lambda\Xi M_p$	ΣNM_p	$\Sigma\Xi M_p$
$\pi\eta$	0^{++}	g	1	–0.2683	–0.5365	0.0000	–0.2683	1/2	0.4646	–0.4646	0.2683	0.2683
			0	–0.4646	0.0000	0.0000	0.4646					
$\pi\pi$	1^{--}	g	1	0.2514	0.4071	0.0553	0.1557	1/2	–0.3802	0.3249	–0.1557	–0.2514
			0	0.3249	–0.0553	0.0553	–0.3802					
$\pi\pi$	1^{--}	f	1	–1.7729	–1.3973	–1.2404	0.3756	1/2	1.8303	–0.5899	–0.3756	1.7729
			0	–0.5899	1.2404	–1.2404	1.8303					
$\pi\rho$	1^{++}	g	1	5.8748	1.7084	5.7973	–4.1665	1/2	–4.3782	–1.4192	4.1665	–5.8748
			0	–1.4192	–5.7973	5.7973	–4.3782					
$\pi\sigma$	1^{++}	g	1	–0.3835	–0.1115	–0.3784	0.2720	1/2	0.2858	0.0926	–0.2720	0.3835
			0	0.0926	0.3784	–0.3784	0.2858					
$\pi\omega$	1^{+-}	g	1	–0.4364	–0.3491	–0.3023	0.0873	1/2	0.4535	–0.1512	–0.0873	0.4364
			0	–0.1512	0.3023	–0.3023	0.4535					

TABLE XI: ESC16 nuclear-bar $\Xi^-\Xi^-(I=1,{}^1S_0)$ and $\Xi^0\Xi^-(I=0,{}^3S_1)$ phases in degrees.

p_Λ	10	50	100	200	300	400	500	600
$T_{\rm lab}$	0.038	0.95	3.77	15.05	36.63	59.22	91.94	129.85
${}^1S_0$	0.04	7.01	17.27	23.71	19.43	11.69	3.05	-5.60
${}^3S_1$	-0.75	-3.77	-7.72	-16.27	-25.36	-34.40	-42.86	-50.43
ϵ_1	0.00	0.03	0.19	0.68	1.02	1.14	1.10	0.94
${}^3P_0$	0.00	0.02	0.21	0.96	1.09	-0.53	-3.96	-8.63
${}^1P_1$	0.00	0.02	0.24	1.64	3.76	15.21	5.13	3.51
${}^3P_1$	-0.00	-0.00	-0.02	0.03	0.06	-0.51	-1.94	-4.11
${}^3P_2$	0.00	0.01	0.10	0.68	1.31	1.14	-0.11	-2.20
ϵ_2	-0.00	-0.00	-0.01	-0.07	-0.23	-0.47	-0.76	-1.07
${}^3D_1$	-0.00	-0.00	-0.01	-0.13	-0.36	-0.80	-1.77	-3.543
${}^1D_2$	0.00	0.00	0.01	0.16	0.74	1.95	3.66	5.49
${}^3D_2$	0.00	0.00	0.03	0.31	0.93	1.66	2.16	2.18
${}^3D_3$	0.00	0.00	0.00	0.04	0.20	0.40	0.37	-0.12

TABLE XII: ESC16 nuclear-bar $\Xi^-\Xi^0$ phases in degrees.

p_Ξ	50	100	200	300	400	500	600	700	800	900
$T_{\rm lab}$	0.95	3.80	15.12	33.79	59.50	91.86	130.42	174.72	224.24	278.51
$^1S_0$	12.65	20.69	23.73	18.44	10.44	1.77	-6.84	-15.11	-22.94	-30.28
$^3S_1$	-3.77	-7.72	-16.27	-25.36	-34.39	-42.85	-50.42	-56.98	-62.54	-67.19
ϵ_1	0.03	0.19	0.68	1.02	1.14	1.10	0.94	0.70	0.40	0.05
$^3P_0$	0.04	0.25	0.99	0.99	-0.78	-4.32	-9.06	-14.41	-19.95	-25.41
$^1P_1$	0.04	0.31	1.78	3.88	5.23	5.03	3.31	0.45	-3.18	-7.29
$^3P_1$	-0.01	-0.02	0.03	0.03	-0.61	-2.10	-4.30	-6.933	-9.75	-12.57
$^3P_2$	0.02	0.13	0.73	1.32	1.09	-0.23	-2.35	-4.90	-7.61	-10.33
ϵ_2	-0.00	-0.01	-0.08	-0.24	-0.48	-0.77	-1.07	-1.36	-1.60	-1.81
$^3D_1$	-0.00	-0.01	-0.13	-0.36	-0.80	-1.77	-3.54	-6.14	-9.42	-13.19
$^1D_2$	0.00	0.01	0.16	0.74	1.94	3.65	5.48	6.98	7.82	7.86
$^3D_2$	0.00	0.03	0.31	0.93	1.66	2.16	2.18	1.64	0.61	-0.77
$^3D_3$	0.00	0.00	0.04	0.20	0.40	0.37	-0.12	-1.11	-2.50	-4.12
ϵ_3	0.00	0.00	0.04	0.15	0.29	0.40	0.48	0.52	0.53	0.51
$^3F_2$	0.00	0.00	0.01	0.07	0.21	0.42	0.55	0.43	-0.11	-1.16

TABLE XIII: I=1/2: ESC16 nuclear-bar $\Lambda\Xi^0$ phases in degrees.

p_Λ	10	50	150	250	350	450	550	650
$T_{\rm lab}$	0.038	0.95	8.53	23.56	45.79	74.88	110.40	151.90
$^1S_0$	0.74	3.58	8.41	8.873	5.93	1.04	-4.82	-10.97
$^3S_1$	-0.53	-2.65	-8.02	-13.50	-18.94	-24.09	-28.78	-32.73
ϵ_1	-0.00	-0.00	-0.12	-0.50	-1.26	-2.47	-4.20	-6.76
$^3P_0$	-0.00	-0.00	-0.06	-0.42	-1.42	-3.20	-5.64	-8.52
$^1P_1$	0.00	0.00	0.09	0.24	0.18	-0.32	-1.34	-2.80
$^3P_1$	-0.00	-0.00	-0.10	-0.47	-1.35	-2.79	-4.70	-6.85
$^3P_2$	0.00	0.00	-0.01	-0.15	-0.64	-1.59	-2.98	-4.68
ϵ_2	-0.00	-0.00	-0.00	-0.01	-0.03	-0.06	-0.08	-0.09
$^3D_1$	0.00	0.00	0.01	0.09	0.36	0.96	2.05	4.15
$^1D_2$	0.00	0.00	0.01	0.10	0.41	1.04	1.99	3.20
$^3D_2$	-0.00	-0.00	-0.00	-0.00	-0.03	-0.14	-0.42	-0.87
$^3D_3$	-0.00	-0.00	-0.00	-0.01	-0.09	-0.35	-0.91	-1.80

TABLE XIV: ESC16 ${}^1S_0, {}^3S_1 - {}^3D_1 (\Lambda\Xi \to \Lambda\Xi, I = 1/2)$ BKS-phase parameters in [degrees] as a function of the laboratory momentum p_Λ in [MeV]. The $\Sigma^0\Xi^0$ and $\Sigma^+\Xi^-$ thresholds are at $p_\Lambda = 689.97$ MeV and $p_\Lambda = 706.47$ MeV respectively.

p_Λ	$\delta({}^1S_0)$	$\rho({}^1S_0)$	$\delta({}^3S_1)$	ϵ_1	$\delta({}^3D_1)$	η_{11}	η_{12}	η_{22}
10	0.74	1.00	–0.53	–0.00	0.00	1.00	0.00	1.00
50	3.58	1.00	–2.65	–0.00	0.00	1.00	0.00	1.00
100	6.52	1.00	–5.31	–0.04	0.00	1.00	0.00	1.00
150	8.41	1.00	–8.02	–0.12	0.01	1.00	0.00	1.00
200	9.16	1.00	–10.75	–0.27	0.03	1.00	0.00	1.00
250	8.87	1.00	–13.50	–0.50	0.09	1.00	0.00	1.00
300	7.72	1.00	–16.24	–0.83	0.19	1.00	0.00	1.00
350	5.93	1.00	–18.94	–1.26	0.36	1.00	0.00	1.00
400	3.65	1.00	–21.56	–1.80	0.61	1.00	0.00	1.00
450	1.04	1.00	–24.09	–2.47	0.96	1.00	0.00	1.00
500	-1.82	1.00	–26.51	–3.26	1.43	1.00	0.00	1.00
550	-4.82	1.00	–28.78	–4.20	2.05	1.00	0.00	1.00
600	-7.90	1.00	–30.89	–5.32	2.90	1.00	0.00	1.00
650	-10.97	1.00	–32.73	–6.76	4.15	1.00	0.00	1.00
700	-13.80	0.990	–34.47	1.20	5.99	0.92	0.31	0.91
750	-17.14	0.972	–38.66	3.64	4.65	0.88	0.30	0.84
850	-23.997	0.956	–45.41	5.34	3.07	0.87	0.28	0.81
950	-30.624	0.945	–51.22	6.21	1.93	0.87	0.28	0.73
1050	-36.967	0.936	–56.42	6.69	0.70	0.87	0.28	0.71
1150	-42.966	0.928	–61.15	6.91	–0.70	0.88	0.28	0.68
1250	-41.319	0.921	–65.53	6.93	–2.26	0.89	0.29	0.66
1350	-35.927	0.915	–69.50	6.81	–4.06	0.89	0.29	0.64
1450	-30.988	0.908	–73.07	6.59	–5.96	0.90	0.29	0.64

TABLE XV: ESC16 ${}^1S_0, {}^3S_1 - {}^3D_1 (\Sigma^0\Xi^0 \to \Sigma^0\Xi^0, I = 1/2)$ BKS-phase parameters in [degrees] as a function of the laboratory momentum p_Σ in [MeV]. The $\Sigma^+\Xi^-$-threshold at $p_\Sigma = 138.15$ MeV.

p_Σ	$\delta({}^1S_0)$	$\rho({}^1S_0)$	$\delta({}^3S_1)$	ϵ_1	$\delta({}^3D_1)$	η_{11}	η_{12}	η_{22}
10	−0.18	1.00	0.44	0.00	0.00	0.99	0.00	1.00
50	−0.85	1.00	2.19	0.01	0.00	0.96	0.00	1.00
100	−1.11	0.99	4.46	0.04	0.01	0.94	0.01	1.00
150	−2.38	0.83	8.14	−0.09	0.09	0.87	0.00	1.00
200	−3.65	0.67	7.38	−0.42	0.19	0.78	0.01	1.00
250	−10.02	0.59	6.01	−0.63	0.33	0.75	0.03	0.99
300	−16.30	0.55	4.24	−0.75	0.49	0.73	0.04	0.98
350	−22.32	0.52	2.12	−0.77	0.67	0.72	0.05	0.97
400	−28.05	0.50	−0.30	−0.69	0.86	0.71	0.07	0.96
450	−33.45	0.49	−2.99	−0.51	1.03	0.70	0.08	0.95
500	−38.52	0.48	−5.93	−0.27	1.20	0.69	0.09	0.93
550	−43.27	0.48	−9.07	0.04	1.34	0.68	0.09	0.91
600	−42.29	0.48	−12.37	0.37	1.46	0.68	0.10	0.89
650	−38.16	0.48	−15.81	0.72	1.56	0.67	0.10	0.87
700	−34.30	0.49	−19.32	1.04	1.64	0.67	0.10	0.85
750	−30.72	0.50	−22.85	1.34	1.68	0.67	0.10	0.83
850	−24.23	0.52	−29.86	1.78	1.63	0.67	0.09	0.80
950	−18.55	0.55	−36.59	2.05	1.28	0.68	0.08	0.76
1050	−13.51	0.58	−42.90	2.21	0.52	0.69	0.07	0.74
1150	−9.84	0.61	−48.69	2.30	−0.72	0.70	0.06	0.72
1250	−5.02	0.64	−53.98	2.39	−2.41	0.71	0.06	0.70
1350	−1.31	0.67	−58.93	2.51	−4.32	0.72	0.05	0.70
1450	1.94	0.70	−63.54	2.62	−6.62	0.74	0.04	0.69

TABLE XVI: I=3/2: ESC16 nuclear-bar $\Sigma^+\Xi^0$ phases in degrees.

p_{Σ^+}	50	150	250	350	450	550	650	750	850	950
$T_{\rm lab}$	1.05	9.42	25.99	50.43	82.28	121.01	166.03	216.72	272.51	332.83
$^1S_0$	12.15	22.97	19.53	10.95	1.04	-8.89	-18.41	-27.33	-35.62	-43.27
$^3S_1$	6.08	11.86	9.42	2.98	-4.90	-13.09	-21.11	-28.73	-35.86	-42.47
ϵ_1	0.09	1.38	3.59	5.99	8.21	10.13	11.75	13.10	14.23	15.16
$^3P_0$	-0.07	-0.97	-2.63	-5.43	-9.75	-15.24	-21.33	-27.53	-33.52	-39.11
$^1P_1$	-0.07	-1.32	-4.55	-9.70	-16.21	-23.39	-30.68	-37.72	-44.28	-50.21
$^3P_1$	0.03	0.41	0.06	-1.69	-4.59	-8.15	-11.96	-15.78	-19.45	-22.90
$^3P_2$	0.01	0.04	-0.23	-1.31	-3.38	-6.19	-9.37	-12.67	-15.93	-19.08
ϵ_2	0.00	0.07	0.20	0.20	0.06	-0.08	-0.15	-0.10	0.05	0.26
$^3D_1$	-0.00	-0.04	-0.20	-0.45	-0.81	-1.37	-2.22	-3.39	-5.29	-7.67
$^1D_2$	-0.00	-0.01	0.25	1.33	3.29	5.65	7.65	8.75	8.73	7.62
$^3D_2$	0.00	0.17	1.07	3.21	6.63	10.63	14.17	16.54	17.55	17.34
$^3D_3$	0.00	0.02	0.18	0.62	1.26	1.82	1.99	1.58	0.53	-1.11
ϵ_3	0.00	0.01	0.11	0.32	0.69	1.23	1.90	2.65	3.44	4.27
$^3G_3$	-0.00	-0.00	-0.01	-0.03	-0.05	-0.03	0.08	0.31	0.72	1.35

TABLE XVII: ESC16*(A) nuclear-bar $\Xi^0\Xi^0$ and $\Xi^-\Xi^0$ phases in degrees.

p_Ξ	50	100	200	300	400	500	600	700	800	900
$T_{\rm lab}$	0.95	3.80	15.12	33.79	59.50	91.86	130.42	174.72	224.24	278.51
$^1S_0$	11.40	18.76	21.45	16.07	8.01	-0.72	-9.36	-17.66	-25.51	-32.86
$^3S_1$	-3.48	-7.15	-15.26	-24.03	-32.81	-40.98	-48.21	-54.35	-59.44	-63.59
ϵ_1	0.03	0.17	0.61	0.88	0.92	0.76	0.48	0.11	-0.35	-0.88
$^3P_0$	0.04	0.25	1.03	1.10	-0.63	-4.15	-8.85	-14.12	-19.50	-24.72
$^1P_1$	0.04	0.31	1.75	3.70	4.72	4.08	1.92	-1.33	-5.28	-9.64
$^3P_1$	-0.00	0.01	0.22	0.46	0.06	-1.30	-3.43	-6.05	-8.893	-11.76
$^3P_2$	0.02	0.15	0.89	1.72	1.72	0.62	-1.29	-3.57	-5.96	-8.30
ϵ_2	-0.00	-0.01	-0.07	-0.23	-0.46	-0.74	-1.04	-1.32	-1.57	-1.78
$^3D_1$	-0.00	-0.01	-0.11	-0.28	-0.62	-1.47	-3.12	-5.63	-8.83	-12.53
$^1D_2$	0.00	0.01	0.17	0.78	2.05	3.83	5.69	7.14	7.89	7.80
$^3D_2$	0.00	0.02	0.30	0.94	1.74	2.36	2.51	2.11	1.23	-0.03
$^3D_3$	0.00	0.00	0.05	0.25	0.53	0.59	0.17	-0.76	-2.10	-3.66
ϵ_3	0.00	0.00	0.04	0.14	0.27	0.37	0.44	0.46	0.45	0.42
$^3F_2$	0.00	0.00	0.01	0.07	0.22	0.45	0.61	0.50	-0.06	-1.14

TABLE XVIII: I=1/2: ESC16*(A) nuclear-bar $\Lambda\Xi^0$ phases in degrees.

p_Λ	10	50	150	250	350	450	550	650
$T_{\rm lab}$	0.038	0.95	8.53	23.56	45.79	74.88	110.40	151.90
$^1S_0$	1.61	7.72	17.17	18.01	14.07	8.05	11.30	-5.35
$^3S_1$	-0.13	-0.69	-2.61	-5.69	-9.74	-14.30	-19.06	-23.84
ϵ_1	-0.00	-0.00	-0.12	-0.47	-1.12	-2.02	-3.11	-4.30
$^3P_0$	0.00	0.01	0.16	0.40	0.31	-0.45	-1.91	-3.86
$^1P_1$	0.00	0.01	0.17	0.47	0.47	-0.20	-1.62	-3.53
$^3P_1$	0.00	0.01	0.13	0.38	0.45	0.05	-0.87	-2.10
$^3P_2$	0.00	0.01	0.22	0.72	1.21	1.32	0.93	0.08
ϵ_2	-0.00	-0.00	-0.00	-0.01	-0.03	-0.05	-0.06	-0.05
$^3D_1$	0.00	0.00	0.01	0.14	0.56	1.43	2.83	4.98
$^1D_2$	0.00	0.00	0.02	0.16	0.62	1.54	2.91	4.59
$^3D_2$	0.00	0.00	0.00	0.05	0.17	0.34	0.48	0.54
$^3D_3$	0.00	0.00	0.00	0.03	0.07	0.03	-0.22	-0.77

TABLE XIX: ESC16*(A) $^1S_0$,$^3S_1$ $-^3D_1(\Lambda\Xi \to \Lambda\Xi, I = 1/2)$ BKS-phase parameters in [degrees] as a function of the laboratory momentum p_Λ in [MeV]. The $\Sigma^0\Xi^0$ and $\Sigma^+\Xi^-$ thresholds are at $p_\Lambda = 689.97$ MeV and $p_\Lambda = 706.47$ MeV respectively.

p_Λ	$\delta(^1S_0)$	$\rho(^1S_0)$	$\delta(^3S_1)$	ϵ_1	$\delta(^3D_1)$	η_{11}	η_{12}	η_{22}
10	1.61	1.00	–0.13	–0.00	0.00	1.00	0.00	1.00
50	7.72	1.00	–0.69	–0.00	0.00	1.00	0.00	1.00
100	13.67	1.00	–1.52	–0.04	0.00	1.00	0.00	1.00
150	17.17	1.00	–2.61	–0.12	0.01	1.00	0.00	1.00
200	18.43	1.00	–4.00	–0.26	0.05	1.00	0.00	1.00
250	18.01	1.00	–5.69	–0.47	0.14	1.00	0.00	1.00
300	16.43	1.00	–7.62	–0.76	0.30	1.00	0.00	1.00
350	14.07	1.00	–9.74	–1.12	0.56	1.00	0.00	1.00
400	11.21	1.00	–11.98	–1.54	0.93	1.00	0.00	1.00
450	8.05	1.00	–14.30	–2.02	1.43	1.00	0.00	1.00
500	4.71	1.00	–16.67	–2.55	2.05	1.00	0.00	1.00
550	1.30	1.00	–19.06	–3.11	2.83	1.00	0.00	1.00
600	–2.09	1.00	–21.45	–3.69	3.77	1.00	0.00	1.00
650	–5.35	1.00	–23.84	–4.30	4.98	1.00	0.00	1.00
700	–8.16	0.981	–26.28	0.10	6.36	0.99	0.17	0.97
750	–11.74	0.945	–28.80	0.36	7.01	0.98	0.17	0.91
850	–19.42	0.912	–33.44	0.08	7.95	0.98	0.19	0.89
950	–26.85	0.892	–37.97	–0.18	9.27	0.97	0.22	0.87
1050	–34.01	0.878	–42.44	–0.37	10.20	0.96	0.23	0.85
1150	–40.80	0.872	–46.81	–0.53	10.48	0.96	0.23	0.83
1250	–42.77	0.873	–51.09	–0.69	10.11	0.95	0.23	0.81
1350	–36.83	0.879	–55.17	–0.84	9.08	0.94	0.23	0.79
1450	–31.51	0.888	–58.93	–0.98	7.57	0.94	0.22	0.78

TABLE XX: ESC16*(A) $^1S_0$,$^3S_1$ $-^3D_1(\Sigma^0\Xi^0 \to \Sigma^0\Xi^0, I = 1/2)$ BKS-phase parameters in [degrees] as a function of the laboratory momentum p_Σ in [MeV]. The $\Sigma^+\Xi^-$-threshold at $p_\Sigma = 138.15$ MeV.

p_Σ	$\delta(^1S_0)$	$\rho(^1S_0)$	$\delta(^3S_1)$	ϵ_1	$\delta(^3D_1)$	η_{11}	η_{12}	η_{22}
10	0.75	1.00	7.96	0.00	0.00	0.99	–0.00	1.00
50	3.86	0.99	36.17	0.00	0.00	0.96	–0.00	1.00
100	9.04	0.98	64.73	0.02	0.02	0.98	–0.01	1.00
150	21.73	0.54	–41.70	–0.03	0.06	0.23	0.05	1.00
200	5.03	0.44	15.37	–1.93	0.23	0.25	0.04	1.00
250	–2.78	0.45	18.87	–2.18	0.41	0.40	0.05	0.99
300	–8.41	0.46	18.07	–2.34	0.67	0.49	0.06	0.99
350	–13.13	0.48	16.00	–2.44	1.01	0.56	0.07	0.98
400	–17.32	0.49	13.32	–2.48	1.43	0.61	0.09	0.97
450	–21.10	0.51	10.27	–2.47	1.92	0.64	0.09	0.96
500	–24.53	0.54	7.00	–2.42	2.48	0.67	0.10	0.94
550	–27.65	0.56	3.58	–2.34	3.09	0.69	0.10	0.93
600	–30.48	0.59	0.07	–2.24	3.74	0.70	0.11	0.91
650	–33.06	0.63	–3.50	–2.15	4.40	0.72	0.10	0.89
700	–35.44	0.66	–7.08	–2.07	5.06	0.72	0.10	0.87
750	–37.59	0.69	–10.65	–2.02	5.66	0.73	0.09	0.85
850	–41.48	0.76	–17.62	–2.02	6.67	0.75	0.07	0.81
950	–44.97	0.82	–24.28	–2.09	7.18	0.76	0.05	0.79
1050	–41.75	0.87	–30.56	–2.18	7.09	0.77	0.03	0.76
1150	–38.59	0.90	–36.40	–2.23	6.32	0.78	0.02	0.75
1250	–35.49	0.93	–41.78	–2.21	4.95	0.79	–0.00	0.74
1350	–32.28	0.95	–46.86	–2.15	3.25	0.80	–0.02	0.74
1450	–29.00	0.96	–51.70	–2.03	1.12	0.81	–0.03	0.74

TABLE XXI: I=3/2: ESC16*(A) nuclear-bar $\Sigma^+\Xi^0$ phases in degrees.

p_{Σ^+}	50	150	250	350	450	550	650	750	850	950
$T_{\rm lab}$	1.05	9.42	25.99	50.43	82.28	121.01	166.03	216.72	272.51	332.83
$^1S_0$	10.77	20.54	16.99	8.37	-1.59	-11.58	-21.14	-30.11	-38.44	-46.11
$^3S_1$	8.64	16.67	14.29	7.58	-0.48	-8.72	-16.68	-24.18	-31.17	-37.62
ϵ_1	0.10	1.42	3.59	5.87	9.93	9.66	11.07	12.21	13.14	13.89
$^3P_0$	-0.06	-0.88	-2.38	-5.03	-9.24	-14.62	-20.56	-26.53	-32.18	-37.31
$^1P_1$	-0.07	-1.25	-4.34	-9.38	-15.84	-23.06	-30.46	-37.67	-44.46	-50.68
$^3P_1$	0.03	0.48	0.31	-1.21	-3.92	-7.32	-11.01	-14.72	-18.29	-21.66
$^3P_2$	0.01	0.09	-0.07	-1.06	-3.08	-5.84	-8.98	-12.20	-15.35	-18.35
ϵ_2	0.00	0.07	0.19	0.19	0.06	-0.09	-0.15	-0.10	0.04	0.23
$^3D_1$	-0.00	-0.04	-0.19	-0.41	-0.72	-1.23	-2.03	-3.22	-4.89	-7.08
$^1D_2$	-0.00	-0.01	0.29	1.44	3.51	5.94	7.95	8.99	8.85	7.62
$^3D_2$	0.00	0.17	1.09	3.32	6.90	11.08	14.80	17.30	18.41	18.27
$^3D_3$	0.00	0.02	0.19	0.67	1.34	1.91	2.04	1.58	0.49	-1.20
ϵ_3	0.00	0.01	0.10	0.31	0.68	1.22	1.89	2.64	3.43	4.24
$^3G_3$	-0.00	-0.00	-0.01	-0.03	-0.04	-0.01	0.12	0.37	0.81	1.45

Acknowledgments

Th.A.R. would like to thank P.M.M. Maessen and V.G.J. Stoks, for their collaboration in constructing the soft-core $S = -2, -3, -4$ OBE-model.

---

[1] M.M. Nagels, Th.A. Rijken, and Y. Yamamoto, Phys. Rev. **C 99**, 044002 (2019).
[2] M.M. Nagels, Th.A. Rijken, and Y. Yamamoto, Phys. Rev. **C 99**, 044003 (2019).
[3] M.M. Nagels, Th.A. Rijken, and Y. Yamamoto, Phys. Rev. **C 102**, 054003 (2020).
[4] V.G.J. Stoks and Th.A. Rijken, Phys. Rev. C **59**, 3009 (1999).
[5] E. Hiyama, T. Motoba, Y. Yamamoto, Progr. Theor. Phys. Suppl. **185** (2010) 1-298.
[6] L. Fabietti *et al*, ALICE-collaboration, CERN-LHC, arXiv:1905.07209 [hep-ex] 2019; arXiv:1910.14407 [hep-ex] 2019.
[7] S. Acharya *et al*, Phys. Rev. Lett. **123**, 112002 (2019).
[8] L. Fabietti, V. Mantovani Sarti, and O. Vázquez Doce, Ann. Rev. Nucl. Part. Sci, **77**, 1-28 (2021).
[9] T. Nagae, Proc. of APPC14, Kuching, Malaysia, 17-22 November 2019.
[10] Y. Fujiwara, Y. Suzuki, and C. Nakamoto, Progress in Particle and Nuclear Physics **58** (2007) 439-520.
[11] N. Ishii, *et al*, arXiv:1702.03495v1 [hep-lat].
[12] T. Doi *et al*, arXiv:1702.01600v2 [hep-lat].
[13] J. Haidenbauer and U.-G. Meissner, arXiv:2201.08238v1 [nucl-th].
[14] M. Isshiki, arXiv:2109.10953 [nucl-ex].
[15] H. Takahashi, et al., Phys. Rev. Lett. **87**, 212502 (2001).
[16] M. Danysz, et al., Nucl. Phys. **49** 121 (1963).
[17] D. J. Prowse, Phys. Rev. Lett. **17** 782 (1966).
[18] E. Hiyama and K. Nakazawa, Ann. Rev. Nucl. Part. Sci, **68**, 131 (2018).
[19] S. H. Hayakawa *et al*, Phys. Rev. Lett. **126**, 062501 (2021)
[20] M. Yoshimoto *et al*, Progr. Theor. Expt. Phys. **2021**, 073D02 (2021).
[21] E. Hiyama, M. Isaka, T. Doi, and T. Hatsuda, arXiv: 2209.06711v1 [nucl-th]
[22] Th.A. Rijken, Phys. Rev. **C73**, 044007 (2006) [arXiv:nucl-th/0603041]
[23] Th.A. Rijken and Y. Yamamoto, Phys. Rev. **C73**, 044008 (2006) [arXiv:nucl-th/0603042]
[24] A. Gal, E.V. Hungerford, and D.J. Miller, Rev. Mod. Phys. **88**, 035004 (2016); Providencia AIP Conf. proc. 2117, 02022 (2019).
[25] L. Tolos and L. Fabietti, Progress in Particle and Nuclear Physics, **112**, 103770 (2020).
[26] S. Nishizaki, Y. Yamamoto, and T. Takatsuka, Progr. Theor. Phys. **105**, 607 (2001); *ibid* **108**, 703 (2002).
[27] R.L. Jaffe, Phys. Rev. Lett. **38**, 195 (1977); **38**, 617(E) (1977).
[28] K. Nakazawa *et al*, Nucl. Phys. **A 835** (2010) 207.
[29] K. Nakazawa *et al*, Progr. Theor. Exp. Phys. **2015**, 033D02.
[30] T. Motoba and S. Sugimoto, Nucl. Phys. **A 835** (2010) 223.
[31] Th.A. Rijken, V.G.J. Stoks, and Y. Yamamoto, Phys. Rev. C **59**, 21 (1999).
[32] P.M.M. Maessen, Th.A. Rijken, and J.J. de Swart, Phys. Rev. C **40**, 2226 (1989).
[33] M.M. Nagels, T.A. Rijken, and J.J. de Swart, Ann. Phys. (N.Y.) **79**, 338 (1973).
[34] J.J. de Swart, Rev. Mod. Phys. **35**, 916 (1963); **37**, 326(E) (1965).
[35] M. Gell-Mann, California Institute of Technology, Report CTSL–20, 1961 (unpublished).

[36] P.A. Carruthers, 'Introductionto unitary symmetry', John Wiley & Sons Inc., New York , 1966.
[37] J.J. de Swart, M.M. Nagels, T.A. Rijken, and P.A. Verhoeven, Springer Tracts Mod. Phys. **60**, 138 (1971).
[38] H.P. Stapp, T. Ypsilantis, and N. Metropolis, Phys. Rev. **105**,302 (1957).
[39] R.A. Bryan, Phys. Rev. C **24**, 2659 (1981); **30** 305 (1984).
[40] S. Klarsfeld, Phys. Lett. **B126**, 148 (1983).
[41] D.W.L. Sprung, Phys. Rev. C **32**, 699 (1985).
[42] A. Kabir and M.W. Kermode, J. Phys. G **13** (1987) 501.